Heat Transport in Molecular Junctions

Dissertation

zur Erlangung des Doktorgrades der Naturwissenschaften

an der Mathematisch-Naturwissenschaftlichen Fakultät

der Universität Augsburg

vorgelegt von

Dipl.-Phys. Fei Zhan

aus Shandong, China

Augsburg, November 2011

1. Gutachter: Prof. Dr. Peter Hänggi
2. Gutachter: Prof. Dr. Sigmund Kohler
Tag der mündlichen Prüfung: 16. Dezember 2011

to my parents

Contents

1. Introduction

Although rudimentary heat engines were already invented and constructed in Antiquity, the first successful commercial engines did not come up until the beginning of 18th century when people began to gain a better understanding of the principles of heat control in the processes involved. Since then, heat engines have played a dominant role in industrial revolution which marked a turning point in human history.

In thermodynamics, energy in the form of heat can be transferred from one system to another one. In a spontaneous process, heat always flows from hot to cold, as is described by the Second Law of Thermodynamics. The Second Law also tells us that it is impossible for a heat engine to convert the whole heat input into mechanical work; and that work applied by an external source is always necessary to make heat flow from cold to hot.

In the solid state realm, heat transport is generally mediated by phonons, being excitations of lattice vibration modes, and electrons. At the same time, phonons, which are traditionally considered as noise source especially in low-temperature physics, might be useful for information processing [1, 2], thus providing an alternative to electronics. In this context, the theoretical design of novel thermal devices such as thermal diodes [3–9], thermal transistors [10, 11], thermal logic gates [12], and thermal memories [13] have been promoted. Accompanying this theoretical progress, solid-state thermal diodes have been realized experimentally with asymmetric nanotubes [14] and semiconductor quantum dots [15].

The fundamental model on which most of the said theoretical works are based is a one-dimensional homogeneous nonlinear lattice connected to a heat bath at both ends. This model has turned out to be an ideal concept for studying the details of heat transport. By harvesting ideas from the field of Brownian motors — devised for particle transport — we pointed out in Refs. [16] and [P1] how heat could be shuttled across a low-dimensional lattice using a Brownian heat engine. In such an engine, a nonvanishing net heat flow can be induced by adiabatically modulating the temperatures of one or both heat baths. Even if the temperature difference between both baths averages to zero over one complete modulation period, specific symmetry breakings ensure the occurrence of this net heat flow. Two different kinds of temperature modulations were proposed in Refs. [16] and [P1], respectively: (i) a symmetric, harmonic ac modulation of the temperature of one heat bath only, and (ii) a simultaneous modulation of the

temperatures of both heat baths. In the latter case, we impose a harmonic mixing with respect to the temperature modulations of both heat baths. This means that the modulations are not only out of phase but also contain both a fundamental harmonic frequency and a second harmonic.

With respect to the field of molecular electronics that has emerged over the last two decades [17–20], the mentioned studies of heat transport are of high importance and interest. In fact, the molecular junction, being an extended molecule connected to two metal leads, constitutes a key hardware element of molecular electronics. It was first proposed as a nanoscale current rectifier by Aviram and Ratner in 1974 [21] and has been considered as an important prototype component for nanotechnologies [22] since then. In 1997, Reed *et al.*, were able to realize this theoretical proposal in an experiment [23]. There, a benzene-1,4-dithiol molecule was connected covalently to two gold electrodes, with two hydrogen atoms substituted by gold atoms. In doing so, they confirmed the existence of only one molecule within a molecular junction, and measured the corresponding current-voltage (IV) characteristics. As a new feature, they discovered the quantized conductance, which stems from the fact that quantum effects become dominant in nanoscale molecular junctions. In later studies, molecular junctions were used as rectifiers [24], pumps [25, 26], switches [27], etc, due to their respective IV characteristics. In general, the structural *stability* of any molecular junction depends sensitively on the heat flow which accompanying the charge transport between the electrodes. For this reason, heat current through molecular junctions constitutes an important physical issue. Despite all this, the phenomenon of heat transport across a molecular junction has so far attracted much less attention in the literature than that of charge transport. This is mainly because the measurement of heat flow experimentally is far from being a straightforward task.

Since the systems of interest are of nanoscale dimensions, the corresponding fluctuations of heat current, i.e., the heat noise, can become quite large. It may occur even in situations where the average heat current vanishes, as in the case of thermal equilibrium. Moreover, the correlation properties of noise or its frequency dependent spectral properties and zero-frequency power spectrum, respectively, are in no way directly related to the mean value of the heat flow itself. With regard to the above mentioned realm of phononics [2], the magnitude of heat current fluctuations is a particular problem because fluctuations may turn out to be deleterious to information processing tasks. It is thus of utmost interest to gain more some insight into the magnitude of heat noise in molecular wire setups. In particular, it would be very useful to have analytical estimates for the power spectral density at hand, even at the expense of needing to restrict onesself to idealized setups only.

The transport of heat across conducting molecular wires, explicitly induced by a difference of the lead temperatures, is a phenomenon which involves electrons,

phonons and their mutual interactions, see e.g. [28–37] and [P2]. Therefore, the definition of heat carried through the wire should be addressed with care, that is, with the need to distinguish between heat transfer mediated by electrons and that mediated by phonons. If no electron-phonon interaction were present, the heat current can be split into two separate contributions mediated by electrons and phonons, respectively. In this scenario, it is also possible to design a Brownian heat engine with the same adiabatic temperature modulation schemes as used in Refs. [16] and [P1]. There, net heat flows can also be created in the absence of any net thermal bias. The new feature of this engine, as compared with those described in Refs. [16] and [P1], is the sensitivity of the electronic heat current to the controlling gate voltage due to the discrete energy levels of the central molecule.

With respect to theoretical modeling, both the electronic and phononic contributions to the heat current through a molecular junction can be described using Landauer-type formulae [38] and [P2]. In the wide-band limit for the conduction bands of the two leads, the Heisenberg equations of motion that are satisfied by the operators related to the electrons in the molecule can be solved with the help of Green functions. Then, important quantities such as the electronic heat current and the power spectral density of the heat current fluctuation are obtained with ensemble averages of the corresponding operators.

The outline of this thesis is as follows. In Chapter 2, we introduce our model which describes the coherent tunneling of electrons across the molecular junction. Then, we briefly outline the method of solving differential equations via Green functions and employ the latter to solve the Heisenberg equations of motion for the system operators. In this way, we obtain the expression of the fluctuation power spectral density in the case of a constant thermal bias. We analyze its dependence on different parameters and compare its properties in the zero-frequency limit with those of the accompanying fluctuation power spectral density of charge current. We find that, even at zero temperature, the power spectral density still shows a frequency-dependence satisfying specific power laws within different frequency ranges.

In Chapter 3, we employ the same model for the electronic subsystem and introduce a quantum mechanical model for the phononic heat current. For each the electron and phonon reservoirs in the leads we introduce two different schemes of temperature modulation in absence of a net thermal bias. Nonetheless, we find that it is possible to generate nonvanishing average heat currents in either case. In what follows, we study the origin of this ratchet effect in detail. Furthermore, we propose and discuss the so-called ratchet "Seebeck" effect.

The thesis is summarized in Chapter 4, where we also present some perspectives of future research.

2. Power Spectral Density of Heat Current Fluctuations

Energy transport mediated by electrons is a process that accompanies an electric current: electron flow (between the leads) across a wire (or junction) carries not only charge but also energy. However, the amount of energy carried by a single electron, unlike its charge, is not constant [39, 40]. In contrast to the studies that examine the average heat flow, much less attention has been paid to the impact of *fluctuations* of heat flow across nanoscale devices. In a prior work [41] heat transport through a ballistic quantum wire has been considered in the Luttinger-liquid limit, by neglecting the discreteness of the wire's energy spectrum. In more recent publications [42,43], the power spectrum density (PSD) of the heat current fluctuations has been derived within scattering theory, under the assumption that electrons are transmitted (reflected) at the same rates, independently of their actual energies. The results of Refs. [42, 43] are distinctive: Heat noise exhibits a well-pronounced frequency dependence even in the zero-temperature limit. These findings highlight the fact that heat current is a process quite different from what one would expect by considering quantum energy transport as mediated by a set of particles (or excitations) bouncing between the leads.

In the following, we take into account the dependence of the transmission coefficient on the incident electron energies. This characteristic constitutes a major extension of the findings of Refs. [42, 43], as is shown further in this chapter. In detail, we consider here an idealized model with one *single* energy level in the molecule, which results in a Lorentzian function for the transmission coefficient. We derive the general expression for the PSD of the heat current fluctuations within the Green function approach [19, 36]. With this result at hand we explore different regimes of electron transport and demonstrate that the heat noise in fact is very different from its electric counterpart.

This chapter is organized as follows: In Section 2.1, we present our idealized model and justify the approximations employed. In Section 2.2, we define the operators for electronic heat current and heat noise. In Section 2.3, we briefly outline the Green function method for solving inhomogeneous differential equations and employ it to solve the Heisenberg equations of motion for operators describing electrons. Then we derive the expression for heat current and heat noise. Especially, we analyze the characteristics of the heat noise in equilibrium.

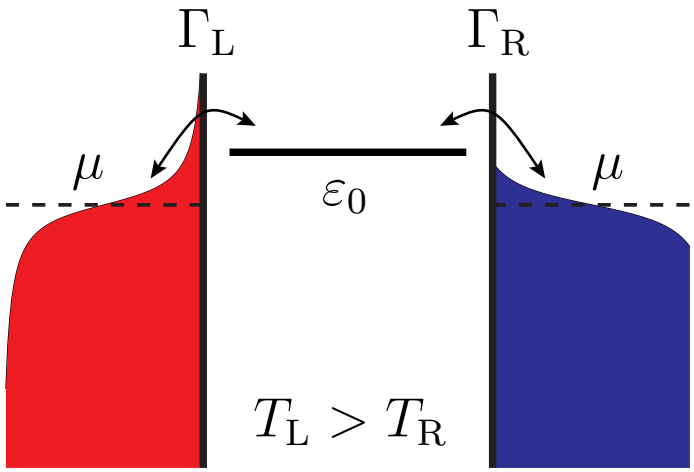

Figure 2.1.: Setup of a molecular junction: two leads each filled with an electron gas are connected by a single orbital ε_0. The coupling strengths are determined by the constants $\Gamma_{\mathrm{L/R}}$. The left lead is prepared at a higher temperature as compared to the right lead, i.e., $T_{\mathrm{L}} > T_{\mathrm{R}}$. The chemical potential μ is the same for both leads, so that no electric current due to a voltage bias is present.

The contents of this chapter can be found in Ref. [P3].

2.1. Model setup for a molecular junction

The molecular junction (MJ) setup, depicted in Figure 2.1, is described by the Hamiltonian

$$H = H_{\mathrm{wire}} + H_{\mathrm{leads}} + H_{\mathrm{contacts}} \,. \tag{2.1}$$

The different terms in this Hamiltonian and approximations employed are described as follows.

2.1.1. Molecular wire

Employing here the tight-binding model, and assuming the wire to be composed of one single orbital only, we can write

$$H_{\mathrm{wire}} = \varepsilon_0 d^\dagger d, \tag{2.2}$$

with the fermionic creation and annihilation operators, $d^\dagger$ and d. The energy level ε_0 can be tuned by applying a gate voltage: a higher gate voltage lowers the energy level and lower gate voltage raises it. This idealized setup enables possible explicit analytical calculations.

2.1.2. The coupling to the electronic leads

The leads are modeled by reservoirs each filled with an ideal electron gas, which occupies the states of conduction bands of the leads. The lead Hamiltonian reads as

$$H_{\text{leads}} = \sum_{\ell q} \varepsilon_{\ell q} c^\dagger_{\ell q} c_{\ell q}, \tag{2.3}$$

where the operator $c^\dagger_{\ell q}(c_{\ell q})$ creates (annihilates) an electron with momentum q in the $\ell =$L (left) or $\ell =$R (right) lead, and $\varepsilon_{\ell q}$ is the corresponding energy.

The lead states with different momentum q or related to different leads are mutually orthogonal, implying $[c_{\ell q}, c^\dagger_{\ell' q'}]_+ = \delta_{ll'}\delta_{qq'}$, where $[A, B]_+ = AB + BA$ is the anti-commutator, and δ is the Kronecker delta. Furthermore, the lead states are orthogonal to the molecular state, implying $[d, c^\dagger_{\ell q}]_+ = 0$.

The temperature on the leads in the following will be assumed constant. As electrons allowed to tunnel into or out of the leads, we thus assume that the electronic distributions in the leads are described by the grand canonical ensembles at the temperatures $T_{\text{L/R}}$ and with chemical potentials $\mu_{\text{L/R}}$. With such idealized electron reservoirs we then obtain

$$\langle c^\dagger_{\ell q} c_{\ell' q'} \rangle = \delta_{\ell\ell'}\delta_{qq'} f_\ell(\varepsilon_{\ell q}), \tag{2.4}$$

where

$$f_\ell(\varepsilon_{\ell q}) = \left[e^{(\varepsilon_{\ell q} - \mu_\ell)/k_{\text{B}}T_\ell} + 1\right]^{-1} \tag{2.5}$$

denotes the Fermi function. The tunneling Hamiltonian

$$H_{\text{contacts}} = \sum_{\ell q} V_{\ell q} c^\dagger_{\ell q} d + h.c. \tag{2.6}$$

mediates the coupling between the wire and the leads. The first term of Eq. (2.6) describes the process of electron tunnelings from the central molecule to either one of the two leads, and the notation $h.c.$ denotes the Hermitian conjugate. The quantities $V_{\ell q}$ are the tunneling matrix elements. In general, the tunneling coupling is characterized by a spectral density [19],

$$\Gamma_\ell(E) = 2\pi \sum_q |V_{\ell q}|^2 \delta(E - \varepsilon_{\ell q}), \tag{2.7}$$

which indicates the coupling strength between the molecular state and a state of energy E in the leads. In the limit where the number of the modes within a constant spectral width goes to infinity, the spectral density becomes a smooth function. It can also be approximated by a sum of Lorentzian functions [44].

If the relevant energy levels are only located in the center of the conduction band, the spectral density is practically energy-independent [19]. Therefore, in

what follows we employ the wide-band limit for the conduction bands of the leads, i.e.,

$$\Gamma_\ell(E) = \Gamma_\ell \ . \tag{2.8}$$

2.1.3. Approximations

In our idealized model, we neglect electron-phonon interactions and electron-electron interactions. This simplification can be justified as follows: for a short wire with a single site the Coulomb interaction due to double occupancy shifts the energy far above the Fermi level, so that its role for thermal transport can be neglected. Likewise, the dwell time of electrons is very short as compared with the relaxation time for electron-phonon interaction in the molecule, for which reason electron-phonon interactions can also be neglected.

2.2. Definitions of heat current and noise

According to Figure 2.1, the heat current is defined as positive when the heat transport proceeds from the left (hotter) lead to the right (colder) lead. In order to obtain a heat current, a temperature difference across the MJ is required. We impose a finite constant temperature difference

$$\Delta T = T_{\rm L} - T_{\rm R} \ , \tag{2.9}$$

and assume identical chemical potentials,

$$\mu_{\rm L} = \mu_{\rm R} = \mu \ , \tag{2.10}$$

for the leads.

As compared with the definition for the charge current, the definition of the heat current is not so obvious. When an electron tunnels out of a lead, the energy E of the tunneling electron leaks into the wire. This energy represents a heat contribution δQ, which in terms of the chemical potential μ reads $\delta Q = E - \mu$, and will finally dissipate in the other lead. Thus, the heat current can be defined as

$$J^{\rm h} = \frac{\sum \delta Q}{\Delta t} \ , \tag{2.11}$$

i.e., the amount of transmitted energy $\sum \delta Q$ across a MJ per unit of time. In the following, we assume that all the electron energies are counted from the chemical potential μ, i. e., we set

$$\mu = 0, \tag{2.12}$$

which results in $\delta Q = E$ (cf. Refs. [37, P2]).

In the following, we employ time-dependent fermionic operators for the electrons. For this reason, we use a Heisenberg description, where all the operators are time-dependent and satisfy Heisenberg equations of motion. Writing the energy operator for the left lead as

$$E_{\rm L}(t) = \sum_q \varepsilon_{{\rm L}q} c^\dagger_{{\rm L}q}(t) c_{{\rm L}q}(t) \ , \tag{2.13}$$

we find that its negative time derivative yields the operator for the heat current:

$$J^{\rm h}_{\rm L}(t) = -\sum_q \frac{2\varepsilon_{{\rm L}q}}{\hbar} {\rm Im}[V_{{\rm L}q} c^\dagger_{{\rm L}q}(t) d(t)]. \tag{2.14}$$

Deriving the above expression, we have employed the Heisenberg equation (2.19) satisfied by the lead electron operators. The average current is obtained by the ensemble average $\langle J^{\rm h}_{\rm L}(t)\rangle$. Since we consider only the heat transport by electrons, we have $\langle J^{\rm h}_{\rm L}(t)\rangle = -\langle J^{\rm h}_{\rm R}(t)\rangle$, due to conservation of energy. Here, as mentioned above, we take the positive direction as from left to right. For this reason, we henceforth may focus on the quantities derived with regard to the left lead.

The heat noise is described by the symmetrized autocorrelation function, i.e.,

$$S^{\rm h}(t,t') = \frac{1}{2}\left\langle [\Delta J^{\rm h}_{\rm L}(t), \Delta J^{\rm h}_{\rm L}(t')]_+ \right\rangle \ , \tag{2.15}$$

with respect to the operator of the heat current fluctuation

$$\Delta J^{\rm h}_{\rm L}(t) = J^{\rm h}_{\rm L}(t) - \langle J^{\rm h}_{\rm L}(t)\rangle \ . \tag{2.16}$$

Here, we have neglected the subscript L for the heat noise. Eq. (2.15) can be rewritten in the form

$$S^{\rm h}(t,t') = \frac{1}{2}\left(\langle J^{\rm h}_{\rm L}(t) J^{\rm h}_{\rm L}(t')\rangle + \langle J^{\rm h}_{\rm L}(t') J^{\rm h}_{\rm L}(t)\rangle - 2\langle J^{\rm h}_{\rm L}(t')\rangle\langle J^{\rm h}_{\rm L}(t)\rangle\right) \ . \tag{2.17}$$

In the asymptotic limit $t \to \infty$, the autocorrelation function depends on the time difference $\tau = t - t'$ only. Its Fourier transform is the *power spectrum density* for the heat noise, obeying

$$\tilde{S}^{\rm h}(\omega) = \tilde{S}^{\rm h}(-\omega) = \int_{-\infty}^{\infty} d\tau e^{i\omega\tau} S^{\rm h}(\tau) \geq 0 \ , \tag{2.18}$$

i.e., $\tilde{S}^{\rm h}(\omega)$ is an even function in frequency and strictly semi-positive, according to the Wiener-Khintchine theorem.

2.3. Methods, results, and discussions

Now the task is to obtain the expectation values that emerge from the definitions of the heat current and autocorrelation function. To this end, we employ the Green function method discussed in Sec. 2.3.1. The annihilation operators of the lead states satisfy the Heisenberg equations of motion

$$\dot{c}_{\ell q}(t) = -\frac{i}{\hbar}\varepsilon_{\ell q}c_{\ell q}(t) - \frac{i}{\hbar}V_{\ell q}d(t)\ , \tag{2.19}$$

for which we obtain the formal solutions

$$c_{\ell q}(t) = c_{\ell q}(t_0)e^{-i\varepsilon_{\ell q}(t-t_0)/\hbar} - \frac{iV_{\ell q}}{\hbar}\int_{t_0}^{t} dt' e^{-i\varepsilon_{\ell q}(t-t')/\hbar}d(t')\ . \tag{2.20}$$

Here, the first term on the right hand side describes the dynamics of the free electrons in the leads, while the second term accounts for the influence of the molecule.

The Heisenberg equation of the molecular annihilation operator is given by

$$\dot{d}(t) = -\frac{i}{\hbar}\varepsilon_0 d(t) - \frac{i}{\hbar}\sum_{\ell q} V^*_{\ell q}c_{\ell q}(t). \tag{2.21}$$

By inserting Eq. (2.20) into Eq. (2.21), we obtain

$$\dot{d} = \frac{i}{\hbar}\varepsilon_0 d(t) - \frac{\Gamma_{\rm L}+\Gamma_{\rm R}}{2\hbar}d(t) + \xi_{\rm L}(t) + \xi_{\rm R}(t), \tag{2.22}$$

where we have defined

$$\xi_\ell(t) = -\frac{i}{\hbar}\sum_q V^*_{\ell q}\exp\left[-\frac{i}{\hbar}\varepsilon_{\ell q}(t-t_0)\right]c_{\ell q}(t_0). \tag{2.23}$$

In addition, we have employed the definition (2.7) and included the wide-band limit.

The quantity defined in Eq. (2.23) is the operator-valued Gaussian noise, which is specified by the expectation values

$$\langle \xi_\ell(t)\rangle = 0 \tag{2.24}$$

$$\langle \xi^\dagger_{\ell'}(t')\xi_\ell(t)\rangle = \delta_{\ell\ell'}\int_{-\infty}^{\infty}\frac{d\varepsilon}{2\pi\hbar^2}e^{-i\varepsilon(t-t')/\hbar}\Gamma_\ell(\varepsilon)f_\ell(\varepsilon). \tag{2.25}$$

It has influence to the molecular states from the leads.

Now the central problem is to solve the inhomogeneous differential equation (2.22). Once we obtain the solution of Eq. (2.22), we obtain also the solution for Eq. (2.20), the current (2.14) and also the power spectrum (2.18) in the end. Before doing so, however, we first briefly outline the Green function method.

2.3.1. Green function method

The Green function method is a helpful tool for solving inhomogeneous differential equations. Assume $\mathcal{L} = \mathcal{L}(x)$ to be a linear differential operator acting on a Hilbert space. Then the Green function $G(x, x')$ is defined as the solution of the differential equation:

$$\mathcal{L}G(x, x') = \delta(x - x') \ , \tag{2.26}$$

where $\delta(x)$ is the Dirac delta function. If this differential equation can be solved, then the solution Green function $G(x, x')$ can be employed to solve the inhomogeneous differential equation of the form,

$$\mathcal{L}u(x) = f(x) \ . \tag{2.27}$$

This can be proved in a few steps [45]. First, we multiply the inhomogeneous term $f(x')$ to both sides of Eq. (2.26) and integrate with respect to x',

$$\int \mathcal{L}G(x, x')f(x')dx' = \int \delta(x - x')f(x')dx' = f(x) \ , \tag{2.28}$$

where the second equation follows from the property of the Dirac delta function. Next, with Eq. (2.27), we have

$$\int \mathcal{L}G(x, x')f(x')dx' = \mathcal{L}u(x) \ . \tag{2.29}$$

Since we have defined $\mathcal{L}$ as a linear operator acting on the variable x only, it can be moved outside of the integral, i.e.,

$$\mathcal{L} \int G(x, x')f(x')dx' = \mathcal{L}u(x) \ . \tag{2.30}$$

This indicates that the solution of Eq. (2.27) is

$$u(x) = \int G(x, x')f(x')dx' \ . \tag{2.31}$$

This equation is also referred to as the Fredholm integral equation.

Then we follow the above Green function approach, which is also employed in Ref. [19], and first solve the following differential equation

$$(\frac{d}{dt} + \frac{i\varepsilon_0}{\hbar} + \frac{\Gamma_{\rm L} + \Gamma_{\rm R}}{2\hbar})G(t - t') = \delta(t - t') \ , \tag{2.32}$$

to find the "kernel", i.e., the Green function $G(t - t')$. After a Fourier transform, we obtain the solution for Eq. (2.32) as

$$G(t) = \theta(t)e^{-i\varepsilon_0 t/\hbar - (\Gamma_{\rm L} + \Gamma_{\rm R})t/2\hbar}, \tag{2.33}$$

where $\theta(t)$ is the Heaviside step function.

In the next step, we calculate the convolution

$$d(t) = \int G(t-t')(\xi_{\rm L}(t') + \xi_{\rm R}(t'))dt' \ , \tag{2.34}$$

which is equivalent to the application of the Fredholm integral equation. Hence the operator for electrons in the molecule in Eq. (2.22) assumes the form

$$d(t) = \sum_{\ell q} V_{\ell q}^* \frac{\exp[-i\varepsilon_{\ell q}(t-t_0)/\hbar]}{\varepsilon_{\ell q} - \varepsilon_0 + i(\Gamma_{\rm L}+\Gamma_{\rm R})/2} c_{\ell q}(t_0). \tag{2.35}$$

With this expression and its Hermitian conjugate, we obtain the occupation number of the molecular energy level ε_0 as

$$\begin{aligned}
\overline{n}_{\varepsilon_0} &= \langle d^\dagger(t) d(t)\rangle \\
&= \sum_{\ell\ell' q q'} \frac{V_{\ell q} V_{\ell' q'}^* \exp[i(\varepsilon_{\ell q} - \varepsilon_{\ell' q})(t-t_0)/\hbar]}{[\varepsilon_{\ell q} - \varepsilon_0 - i(\Gamma_{\rm L}+\Gamma_{\rm R})/2][\varepsilon_{\ell' q'} - \varepsilon_0 + i(\Gamma_{\rm L}+\Gamma_{\rm R})/2]} \langle c_{\ell q}^\dagger(t_0) c_{\ell' q'}(t_0)\rangle \\
&= \sum_{\ell q} \frac{|V_{\ell q}|^2 f_\ell(\varepsilon_{\ell q})}{(\varepsilon_{\ell q} - \varepsilon_0)^2 + (\Gamma_{\rm L}+\Gamma_{\rm R})^2/4} \ ,
\end{aligned} \tag{2.36}$$

where from the first step to the second step, we have employed the ensemble average, Eq. (2.4). We find that this occupation number is determined first by the Fermi function of the leads weighted by the tunneling matrix elements $V_{\ell q}$ and the difference between the energy levels of the lead states and that of the molecular energy level. However, this occupation number is time-independent, since there is no time-dependent external field present. The same also holds true for the average current in the next subsection.

Substituting Eq. (2.35) into Eq. (2.20), we obtain for the operators in the leads

$$\begin{aligned}
c_{\ell q}(t) = {} & c_{\ell q}(t_0) e^{-i\varepsilon_{\ell q}(t-t_0)/\hbar} \\
& + \sum_{\ell' q'} \frac{V_{\ell q} V_{\ell' q'}^* e^{-i\varepsilon_{\ell' q'}(t-t_0)/\hbar}}{\varepsilon_{\ell' q'} - \varepsilon_0 + i(\Gamma_{\rm L}+\Gamma_{\rm R})/2} c_{\ell' q'}(t_0) B[\varepsilon_{\ell' q'} - \varepsilon_{\ell q}].
\end{aligned} \tag{2.37}$$

where we have defined

$$B(E) = \mathcal{P}\left(\frac{1}{E}\right) - i\pi\delta(E), \tag{2.38}$$

and $\mathcal{P}$ denotes the integral principal value; see Appendix A for details. When deriving Eq. (2.37) we have assumed that $t_0 \to -\infty$. From this expression we conclude that the first term represents the free evolution of lead electrons while the second term describes the influence of the molecule.

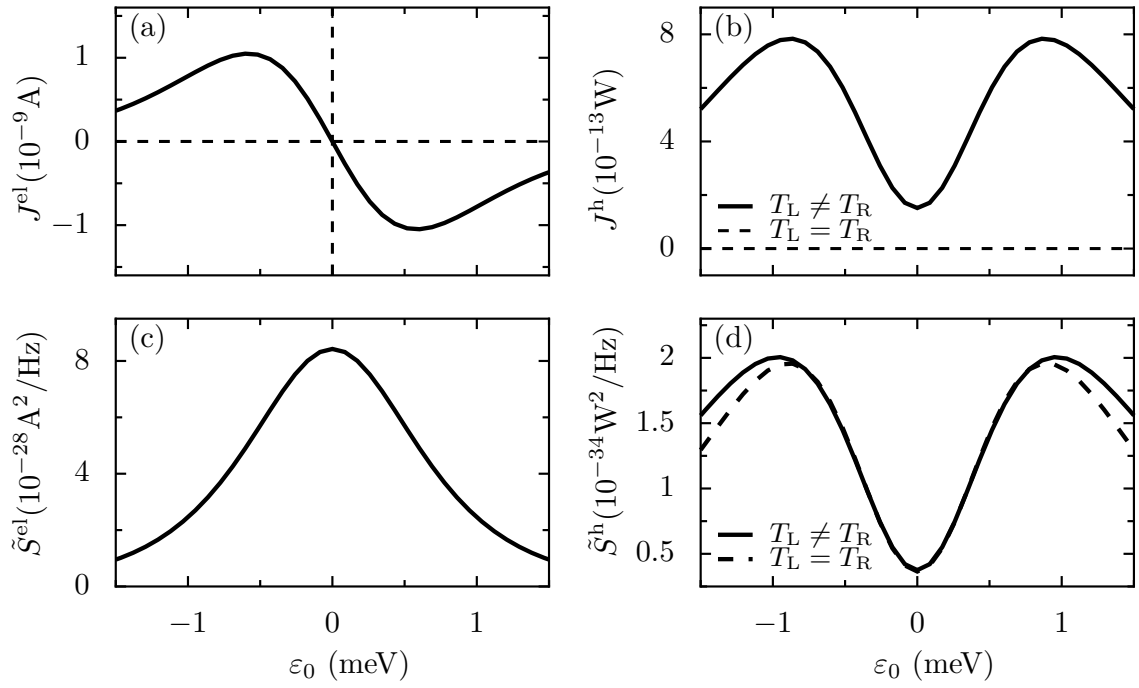

Figure 2.2.: Currents (top row) and zero-frequency components of power spectral densities of accompanying noises (bottom row) for charge (left column) and heat (right column) transport through the single-orbital wire as functions of orbital energy for $\Gamma = 0.1$ meV. The remaining parameters are $T_{\mathrm{L}} = 5.2$ K, $T_{\mathrm{R}} = 3.2$ K (solid lines). For equal chemical potentials $\mu_{\mathrm{L}} = \mu_{\mathrm{R}} = 0$ the heat flow in panel (b) vanishes for equal temperatures $T_{\mathrm{L}} = T_{\mathrm{R}}$; its noise intensity in equilibrium at the temperature $T_{\mathrm{L}} = T_{\mathrm{R}} = 4.2$ K is depicted versus the orbital energy ε_0 by the dashed line in panel (d).

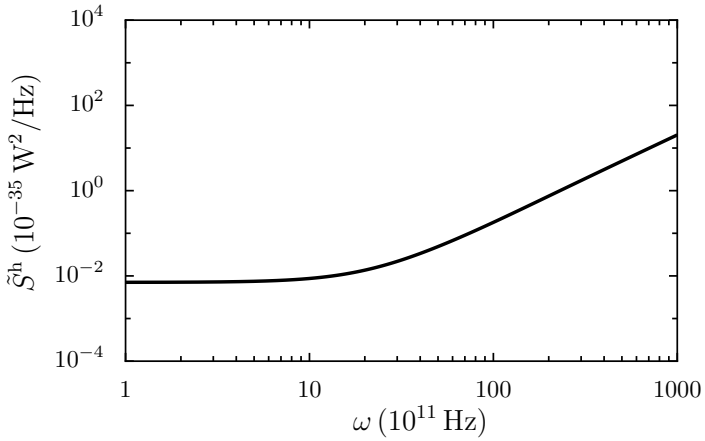

Figure 2.3.: Power spectral density of the heat noise as a function of the frequency ω at temperatures $T_{\rm L} = 6\,{\rm K}, T_{\rm R} = 2\,{\rm K}$. The other parameters are $\varepsilon_0 = 0$ and $\Gamma = 0.1$ meV.

2.3.2. Heat current

With Eq. (2.35) and Eq. (2.37) at hand, we calculate the heat current and heat noise according to the definitions (2.14) and (2.18), and take the ensemble average, according to Eq. (2.4). For the heat current, we obtain a Landauer-type formula [35,37–39], which reads as,

$$\langle J^{\rm h}(t)\rangle := J^{\rm h} = \frac{1}{2\pi\hbar}\int_{-\infty}^{\infty} dE E\mathcal{T}(E)[f_{\rm L}(E) - f_{\rm R}(E)]\;, \tag{2.39}$$

where the transmission coefficient

$$\mathcal{T}(E) = \frac{\Gamma_{\rm L}\Gamma_{\rm R}}{(E-\varepsilon_0)^2 + \Gamma^2}\;, \tag{2.40}$$

being of Breit-Wigner form, is energy-dependent and assumes a Lorentzian shape. We henceforth consider only a symmetric coupling between the wire and the leads, which implies $\Gamma_{\rm L} = \Gamma_{\rm R} = \Gamma$.

The nonlinear electric Seebeck current reads similar to Eq. (2.39), except that the energy multiplier E in the integral on the right-hand side of Eq. (2.39) is replaced by the charge unit e, i.e.,

$$\langle J^{\rm el}(t)\rangle := J^{\rm el} = \frac{e}{2\pi\hbar}\int_{-\infty}^{\infty} dE \mathcal{T}(E)[f_{\rm L}(E) - f_{\rm R}(E)]\;. \tag{2.41}$$

This apparently small difference changes, however, the physics of the transport across the wire, because this multiplier inverts the symmetry of the integral.

Namely, the Seebeck current is an antisymmetric function of the orbital energy and vanishes when the orbital energy level is aligned to the chemical potentials of the leads as indicated in Figure 2.2(a). By contrast, the heat current is a symmetric function of the orbital energy and acquires a nonzero value at $\varepsilon_0 = 0$, see Figure 2.2(b).

2.3.3. The spectrum of heat fluctuations

Upon combining Eq. (2.18) and Eq. (2.14), we finally arrive at the following expression for the PSD of electronic heat noise:

$$\begin{aligned}\tilde{S}^{\mathrm{h}}(\omega;T_{\mathrm{L}},T_{\mathrm{R}}) = \sum_{\pm}\int_{-\infty}^{\infty}\frac{dE}{4\pi\hbar}\Bigg\{\Bigg[&\left(E\pm\frac{\Omega}{2}\right)^2\mathcal{T}(E)\mathcal{T}(E\pm\Omega)\\ &+\frac{\Gamma_{\mathrm{L}}^2\left[E(E-\varepsilon_0)-(E\pm\Omega)(E\pm\Omega-\varepsilon_0)\right]^2}{\left[(E-\varepsilon_0)^2+\Gamma^2\right]\left[(E\pm\Omega-\varepsilon_0)^2+\Gamma^2\right]}\Bigg]f_{\mathrm{L}}(E)\overline{f}_{\mathrm{L}}(E\pm\Omega)\\ &+\left(E\pm\frac{\Omega}{2}\right)^2\mathcal{T}(E)\mathcal{T}(E\pm\Omega)f_{\mathrm{R}}(E)\overline{f}_{\mathrm{R}}(E\pm\Omega)\\ &+[E^2\mathcal{R}(E)\mathcal{T}(E\pm\Omega)\mp\frac{1}{2}E\Omega\mathcal{T}(E)\mathcal{T}(E\pm\Omega)\\ &+\left(E\pm\frac{\Omega}{2}\right)\left(\pm\frac{\Omega}{2}\right)\frac{\Gamma_{\mathrm{L}}^2\mathcal{T}(E\pm\Omega)}{(E-\varepsilon_0)^2+\Gamma^2}]f_{\mathrm{L}}(E)\overline{f}_{\mathrm{R}}(E\pm\Omega)\\ &+[(E\pm\Omega)^2\mathcal{R}(E\pm\Omega)\mathcal{T}(E)+(E\pm\Omega)\left(\pm\frac{\Omega}{2}\right)\mathcal{T}(E)\mathcal{T}(E\pm\Omega)\\ &+\left(E\pm\frac{\Omega}{2}\right)\left(\mp\frac{\Omega}{2}\right)\frac{\Gamma_{\mathrm{L}}^2\mathcal{T}(E\pm\Omega)}{(E-\varepsilon_0)^2+\Gamma^2}]f_{\mathrm{R}}(E)\overline{f}_{\mathrm{L}}(E\pm\Omega)\Bigg\}, \end{aligned}\tag{2.42}$$

where $\Omega \equiv \hbar\omega$, $\overline{f} \equiv 1-f$, and $\mathcal{R}(E) \equiv 1-\mathcal{T}(E)$ is the reflection coefficient.

In Figure 2.3, we depict the dependence of the PSD of heat noise on frequency at temperatures $T_{\mathrm{L}} = 6\,\mathrm{K}, T_{\mathrm{R}} = 2\,\mathrm{K}$. We find that the PSD obeys different power laws in different frequency regions and increases monotonically.

Moreover we find that the spectral density Γ of the wire-lead coupling can change the dependence of the PSD of heat noise on the parameters. In Figure 2.4, for instance, we depict the PSD of heat noise as a function of the temperature difference ΔT in the case of weak and strong wire-lead couplings. With weak coupling, the PSD is smaller by one order of magnitude and only slightly depends on ΔT; whereas it increases very fast with ΔT when the coupling is very strong. According to Eq. (2.40), the transmission coefficient becomes wider when Γ is larger, such that more electrons, whose energies deviate stronger from the chemical potential, are allowed to transport across the MJ. Therefore, the PSD is large and depends sensitively on ΔT.

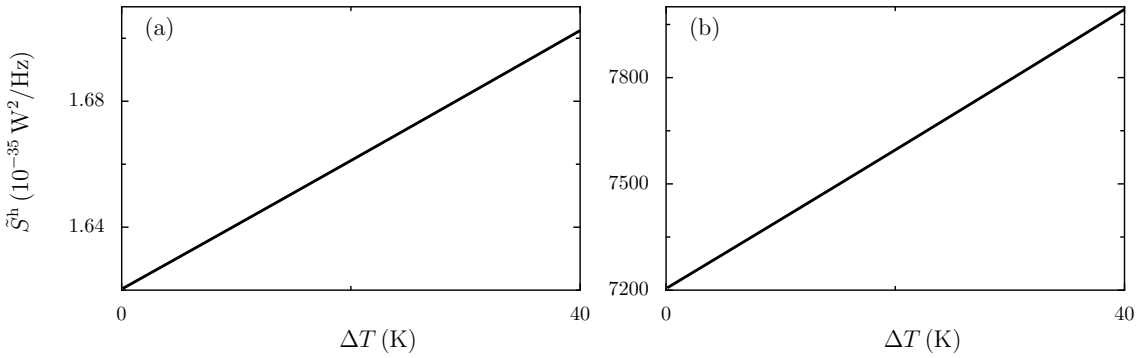

Figure 2.4.: Power spectral density of heat noise at frequency $\omega = 2.16 \times 10^{13}\,\mathrm{Hz}$ (which is the Debye cut-off frequency of gold) as a function of temperature difference with (a) weak molecule-wire coupling $\Gamma = 0.1\,\mathrm{meV}$ or (b) strong molecule-wire coupling $\Gamma = 10\,\mathrm{meV}$. The other employed parameters are $T_{\rm R} = 300$ K and $\varepsilon_0 = 0$.

At $\omega = 0$, the heat noise power simplifies considerably, assuming the appealing form

$$\tilde{S}^{\rm h}(\omega = 0; T_{\rm L}, T_{\rm R}) = \frac{1}{2\pi\hbar}\int_{-\infty}^{\infty} dE E^2 [\mathcal{T}(E)[f_{\rm L}(E)[1 - f_{\rm L}(E)] + f_{\rm R}(E)[1 - f_{\rm R}(E)]] + \mathcal{T}(E)[1 - \mathcal{T}(E)][f_{\rm L}(E) - f_{\rm R}(E)]^2] \,. \tag{2.43}$$

This main result is in agreement with a prediction conjectured in Ref. [41]. The first term in the integral is responsible for the effect of the thermal agitation, i.e., thermal noise. Apart from the thermal noise, the second term corresponds to the noise due to the discreteness of heat carried by the electrons, as compared to shot noise for electronic current. Here, noise stemming from an individual incident electron being transmitted or not is called "partition noise" [46]. This can be justified by the fact that the noise is absent if the electron is definitely transmitted, $\mathcal{T} = 1$, or definitely reflected, $\mathcal{T} = 0$.

The distinct difference between Eq. (2.43) and the PSD of the fluctuations of the nonlinear, accompanying Seebeck electric current, which reads as [19, 46],

$$\tilde{S}^{\rm el}(\omega = 0; T_{\rm L}, T_{\rm R}) = \frac{e^2}{2\pi\hbar}\int_{-\infty}^{\infty} dE [\mathcal{T}(E)[f_{\rm L}(E)[1 - f_{\rm L}(E)] + f_{\rm R}(E)[1 - f_{\rm R}(E)]] + \mathcal{T}(E)[1 - \mathcal{T}(E)][f_{\rm L}(E) - f_{\rm R}(E)]^2]. \tag{2.44}$$

is the factor E^2 instead of e^2, as given in front of the integral in Eq. (2.43). Although this distinction appears minor, it leads to a tangible difference in a two-parameter dependence of the noise PSDs, $\tilde{S}[\varepsilon_0, \Gamma]$, as depicted in Figure 2.5, also

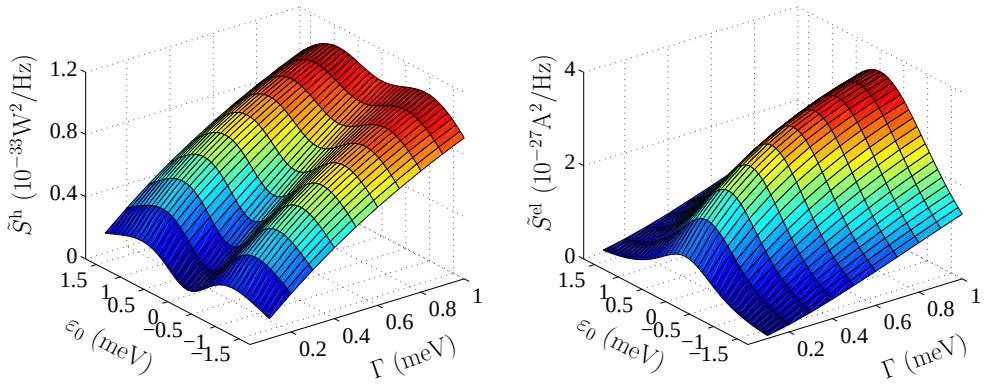

Figure 2.5.: Power spectral density of the heat noise at frequency $\omega = 0$, (left panel) and power spectral density of the electric noise (right panel) as functions of the wire site energy ε_0 and wire-lead coupling strength Γ. The parameters employed are $T_0 = 4.2$ K and $\Delta T = 2$ K.

see Figure 2.2. The zero-frequency component of PSDs for both heat and electric noise increases with increasing coupling strength Γ, with the latter controlling the transmission probability. However, when the orbital level ε_0 is tuned in resonance to the chemical potential, the two expressions reveal different properties, as depicted in Figures 2.5 and 2.2. While the electric PSD at $\omega = 0$ exhibits a maximum at $\varepsilon_0 = 0$, its heat counterpart possesses a local minimum at this point.

This difference originates from the salient fact that the two transport mechanisms for charge and the energy are not equivalent. The electric current is quantized by the electron charge e. By contrast, the energy carried by the electron is not quantized and may principally assume an arbitrary value. The main contribution to the electron flow across the wire stems from the electrons occupying energy levels that are situated around the chemical potential μ.

Since the interaction between the leads and the molecule is weak, it only slightly perturbs the Fermi distributions, which possess strongly nonuniform profiles around $\mu = 0$. Electrons of different energies contribute differently to the heat transport, but the Fermi distribution only allows for finite number of electrons per energy level: i.e., just one electron in the case of spinless electrons, or two in the case of electrons with spin. Therefore, the electrons of given energy can move through the wire only when the corresponding level of the destination lead can host them.

When ε_0 deviates from the chemical potential, less and less electrons participate in the transport, i.e., the flow of electrons becomes reduced. Since both the electric current and the electric noise are insensitive to the electron energies, they both decrease with increasing $|\varepsilon_0|$. A different scenario applies to heat transport:

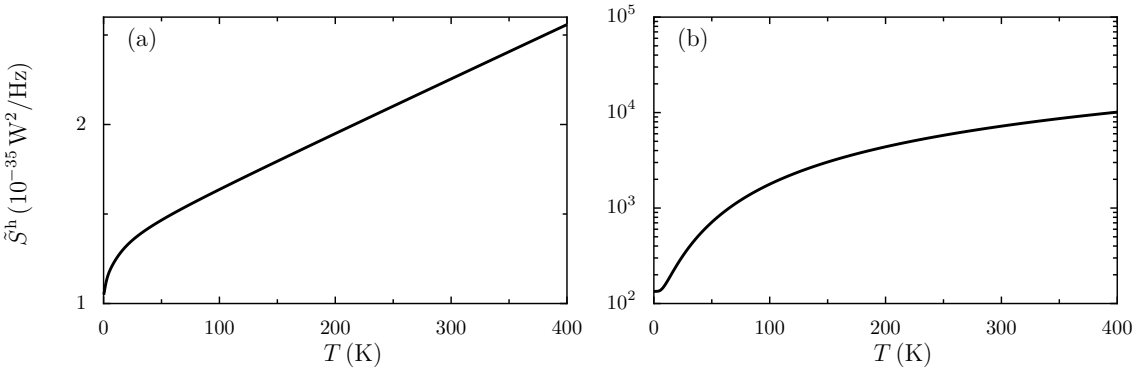

Figure 2.6.: At equilibrium, $T_{\rm L} = T_{\rm R} = T$, the power spectral density of heat noise as a function of the temperature T with $\omega = 2.16 \times 10^{13}\,{\rm Hz}$ with (a) weak molecule-wire coupling $\Gamma = 0.1\,{\rm meV}$ or (b) strong molecule-wire coupling $\Gamma = 10\,{\rm meV}$. The on-site energy is chosen as $\varepsilon_0 = 0$.

the deviation from the chemical potential increases the probability that successive electrons carry different energies. This, in turn, leads to an increase of heat noise. With a further deviation of the orbital energy from the chemical potential, the occupancy difference $f_{\rm L}(E) - f_{\rm R}(E)$ decreases monotonically and, as a consequence, the strength of heat noise decreases.

2.3.4. Equilibrium heat fluctuations at $\mathbf{T_L = T_R}$

Next let us focus on the equilibrium properties of heat noise, i.e., the situation when the two lead temperatures are equal, $T_{\rm L} = T_{\rm R}$. In this case the average heat flow vanishes identically, but not its fluctuations. The zero-frequency spectra of both the heat and electric noise, i.e., the corresponding power spectra increase with the increase of the coupling Γ, since it increases the transmission coefficient. The noise intensities are different from zero, however, even at equilibrium, see Figure 2.2(d).

In Figure 2.6, we depict the dependence of the PSD of heat noise on temperature at $\omega \neq 0$. Its increase with temperature is much faster for stronger coupling Γ [see panel (b)]. We also observe that the PSD does not vanish at absolute zero temperature, where $T_{\rm L} = T_{\rm R} = 0$. The reason for this behavior is more subtle. It has been pointed out in Ref. [43] that the presence of such heat noise violates the fluctuation-dissipation theorem (FDT). In fact, a temperature difference $\triangle T$ does not induce any thermal gradient. Therefore, there is no force which is conjugate to the heat current, and the process is out of the validity region of the FDT. This 'evasion' of the FDT is fully active in the zero-temperature limit, where the PSD of heat noise still depends on the frequency. This dependence is due to quantum

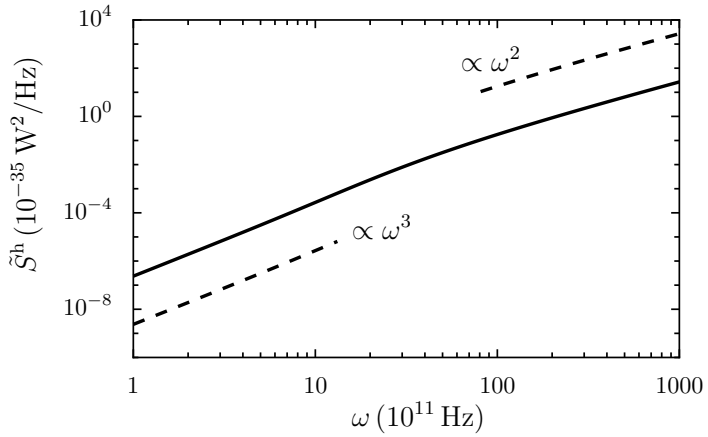

Figure 2.7.: At zero-temperature, $T_{\rm L} = T_{\rm R} = 0$, the dependence of power spectral density of heat noise versus frequency ω exhibits different power-law behaviors (dashed lines) for ω sampling intermediate values (proportional to ω^3) as compared to the large frequency limit $\omega \to \infty$(proportional to ω^2). The other parameters are $\varepsilon_0 = 0$ and $\Gamma = 0.1\,{\rm meV}$.

fluctuations, the virtual transitions of electrons directly from lead to lead [42, 43]. The Fermi distribution equals the Heaviside step function in this case. Thus, the contributions to the integrand in Eq. (2.42) only stem from the interval $[-\Omega,\ 0]$ (note that we henceforth assume $\Omega > 0$). After integration of Eq. (2.42), we find the central result for the frequency dependent PSD as

$$\tilde{S}^{\rm h}(\omega, T_{\rm L} = T_{\rm R} = 0) = \frac{\Gamma}{4\pi\hbar}\left\{\left[(2\Omega)^2 - 2\Gamma^2\right]\arctan\left(\frac{\Omega}{\Gamma}\right) + 2\,\Omega\Gamma\left[1 + \log\left(\frac{\Gamma^4}{\left(\Omega^2+\Gamma^2\right)^2}\right)\right]\right\}, \tag{2.45}$$

where $\Omega = \hbar\omega$. In the limit $\Gamma \to \infty$ the zero-temperature PSD thus scales with frequency as $\tilde{S}^{\rm h}(\omega) \propto \omega^3$. This is in full agreement with the results obtained in Refs. [42, 43], where such an asymptotic behavior has been found to be uniform throughout the whole frequency region. However, such a cubic scaling is no longer given when Γ is finite: the second term on the right-hand side of Eq. (2.45) introduces a linear cutoff in the limit $\omega \to 0$, so that $\tilde{S}^{\rm h}(\omega) \propto \omega$. In distinct contrast, in the high-frequency region, the first term on the right-hand side of Eq. (2.45) dominates. As a result, the PSD (2.45) approaches a square-law asymptotic dependence, $\tilde{S}^{\rm h}(\omega) \propto \omega^2$, see Figure 2.7.

2.4. Summary

Using the Green function formalism, we have investigated the electronic heat transport with our focus being the heat current fluctuations for a setup composed of a single orbital molecular wire. The dependence of the heat noise on the orbital energy ε_0 and the lead-wire coupling strength Γ is qualitatively different from that of the accompanying electric current noise. In the zero-temperature limit the spectrum of the heat noise obeys two distinctive asymptotic behaviors, the low-frequency or the high-frequency regime. It is evident that the particular square-law shape of the PSD in the high-frequency region is due to the Lorentzian shape of the transmission coefficient, $\mathcal{T}(E)$. Yet the general effect would remain for any choice of the coefficient in the form of a localized, bell-shaped function: the noise spectrum will deviate from a cubic power-law asymptotic behavior upon entering the high-frequency region. There is an intriguing perspective to apply an external periodic perturbation to the orbital energy with the goal to control the spectral properties of the heat noise, similar to electronic shot-noise control in ac-driven nanoscale conductors [47]. This idea can be realized, for example, by exposing the molecular wire to strong laser radiation [48] or by a direct modulations of the gate voltage. We conjecture that the role of laser radiation may give rise to novel phenomena that could be explored further by combining a Floquet theory for the driven system with the nonequilibrium Green function formalism [19,39,47].

As emphasized in the introduction, only the electron subsystem has been considered here. A more realistic model of heat transport in real MJs would necessarily involve the difficulty of electron-electron and electron-phonon interactions [37]. As reasoned further in the introduction, the electronic heat transport may dominate in certain situations so that the measured heat noise can be attributed approximately to the electronic component only. All in all, a unified approach, which would include both the electron and the phonon subsystems as well as the effects of their mutual interactions remains a future challenge, although several models in this direction for the heat current (but not the heat PSD) have been provided recently [32,35,37]).

3. Molecular Junctions Acting as Quantum Heat Ratchet

In recent years, we have witnessed the development of nano-devices based on molecular wires [17–20, 49]. One of their essential features is that the electric current through them can be effectively controlled. One approach to such transport control is based on conformational changes of the molecule [50–52]. Another scheme relies on the dipole interaction between the molecular wire and a tailored laser field [48, 53–56]. A further approach employs gate voltages acting on the wire [57–59]. The latter allows a transistor-like control which has already been demonstrated experimentally [60–62]. Meanwhile, the heat transport mediated by the electrons should be treated on an equal footing, due to its importance on the stability of electronic circuit. In Chapter 2, we have demonstrated the characteristic of the electronic heat current and its fluctuations in the case of a constant thermal bias. The problem remains of how one can control the heat current by modulating specific parameters of the investigated system.

In general, heat transport through a molecular junction (MJ) involves the combined effect of electron as well as phonon transfer processes. Control of phonon transport is much more complicated since the phonon number is not conserved. Nevertheless, the field of phononics, i.e., control and manipulation of phonons in nanomaterials, has emerged [1]. This includes functional devices, such as thermal diodes [3–9], thermal transistors [10, 11], thermal logic gates [12], and thermal memories [13] based on the presence of a static temperature bias. The corresponding theoretical research has been accompanied by experimental efforts on nanosystems. In particular, solid-state thermal diodes have been realized with asymmetric nanotubes [14] and with semiconductor quantum dots [15].

By harvesting ideas from the field of Brownian motors [63–67] — originally devised for particle transport — we have proposed a classical Brownian *heat engine* to rectify and steer heat current in nonlinear lattice structures [16, P1]. In the absence of any net non-equilibrium bias, a non-vanishing net heat flow can be induced by unbiased, temporally alternating bath temperatures in combination with nonlinear interactions among neighboring lattice sites. This so obtained directed heat current can be readily made reverse its direction. If, in addition, a thermal bias across the molecule is applied, a heat current can be directed even against the external thermal bias. This setup is rather distinct from adiabatic and

nonadiabatic electron heat pumps which involve photon-assisted transmission and reflection processes in presence of irradiating photon sources [19, 39, 68].

In this chapter, we investigate the possibility of steering heat through a MJ in the presence of a gating mechanism. In doing so, the bath temperatures of adjacent leads are subjected to slow, time-periodic modulations. Both the electronic and the phononic heat current are considered, as sketched in Figure 3.1. The electronic subsystem has been considered in Chapter 2, where we have modeled it using Landauer-type formula.

A finite directed ratchet heat current requires breaking reflection symmetry. This can be achieved by spatial asymmetries in combination with non-equilibrium fields [63–67] or in a purely dynamical way [69–73]. In this work we focus on an unbiased temporal temperature variation in the connecting leads.

This chapter is organized as follows: In Section 3.1, we specify the physical assumptions and introduce our model together with the basic theoretical concepts for directing heat current across a short, gated MJ formed by a harmonically oscillating molecule. In Section 3.2, we propose two schemes of temperature modulation in the absence of net thermal bias: (i) the temperature is modulated in one lead only, and (ii) temperatures of both leads are modulated periodically, but in an asymmetrical way, i.e., with a mutual phase of π. In Section 3.5, we present the results. We find that we can get nonzero average heat current with both schemes of temperature modulation. For case (ii), since the leading term of the heat current is only of third order in the driving amplitudes, the overall rectification is weaker as compared with case (i) where the heat flux starts out at second order in the driving amplitude. The scheme of case (ii) with its symmetric static parameters, however, provides a more efficient control scenario: The direction of the resulting heat current can be readily reversed either by a gate voltage or by adjusting the relative phase shift within the signal of harmonic mixing for the temperature modulation. In Section 3.6, we discuss the origin of the ratchet effect. Finally, we present the *ratchet Seebeck effect* in Section 3.7.

3.1. Model of the molecular junction

Based on the introduction part of this chapter, the total Hamiltonian can be separated into an electron part and a phonon part, i.e.,

$$H = H^{\mathrm{el}} + H^{\mathrm{ph}} \,, \tag{3.1}$$

each of which consists of a wire contribution, a lead contribution, and an interaction term between the former two contributions, such that

$$H^{\mathrm{el(ph)}} = H^{\mathrm{el(ph)}}_{\mathrm{wire}} + H^{\mathrm{el(ph)}}_{\mathrm{leads}} + H^{\mathrm{el(ph)}}_{\mathrm{contacts}} \,. \tag{3.2}$$

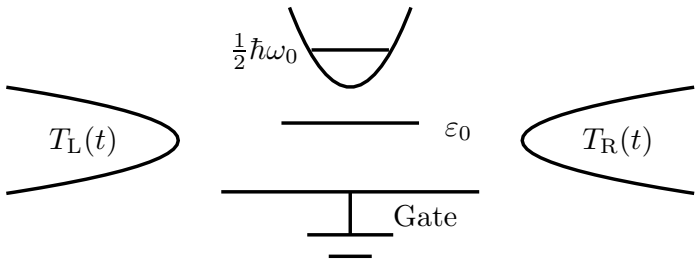

Figure 3.1.: Setup of a molecular junction whose electronic level ε_0 can be gated, while the vibrational frequency ω_0 is fixed. The lead temperatures $T_{\mathrm{L(R)}}(t)$ are subjected to time-periodic modulations.

The Hamiltonian H^{el} of the electronic subsystem is given in Eq. (2.1) in Section. 2.1.

For the phononic subsystem of the Hamiltonian, we only consider one mode of the molecular oscillations. This phonon mode is represented by a harmonic oscillator, yielding the Hamiltonian

$$H^{\mathrm{ph}}_{\mathrm{wire}} = \frac{P^2}{2M} + \frac{1}{2}M\omega_0^2 Q^2\,, \tag{3.3}$$

where Q and P are the position and the momentum operators, respectively; M is the atom mass and ω_0 the single characteristic phonon frequency of the wire. The molecule can perform two kinds of simple periodic displacements: vibration and oscillation [29] (certainly there are other possible eigenmodes, e.g., rocking, twisting, wagging, and scissoring, but these are not interesting in the present context). A vibration is equivalent to an internal stretching displacement, keeping the center of the mass at rest; while during an oscillation, the molecule moves as a whole. In this chapter, we only consider vibrations, assuming there is an internal bond structure of the molecule.

The phonon bath and its bilinear coupling to the wire system are described by

$$H^{\mathrm{ph}}_{\mathrm{leads}} + H^{\mathrm{ph}}_{\mathrm{contacts}} = \sum_{\ell,k}\left\{\frac{p^2_{\ell k}}{2m_\ell} + \frac{m_\ell\omega^2_{\ell k}}{2}\left(x_{\ell k} - \frac{g_\ell Q}{m_\ell\omega_{\ell k}}\right)^2\right\}, \tag{3.4}$$

where $x_{\ell k}, p_{\ell k}, \omega_{\ell k}$ are the position and momentum operators, and frequencies associated with the bath degrees of freedom, respectively; m_ℓ are the masses and $g_\ell = g_{\mathrm{L}} = g_{\mathrm{R}} = g$ represent symmetric phonon wire-lead coupling strengths for the left and right lead $\ell = \mathrm{L}, \mathrm{R}$. The position and momentum operators can be expressed in terms of the phononic creation and annihilation operators, i.e.,

$$x_{\ell k} = \sqrt{\hbar/2m_\ell\omega_{\ell k}}(a^\dagger_{\ell k} + a_{\ell k}) \tag{3.5}$$

and

$$p_{\ell k} = i\sqrt{\hbar m_\ell \omega_{\ell k}/2}(a^\dagger_{\ell k} - a_{\ell k}) \; . \tag{3.6}$$

In thermal equilibrium, the density matrices for the leads read as

$$\rho_\ell = e^{-(H^{\rm ph}_\ell + H^{\rm el}_\ell - \mu_\ell N_\ell)/k_{\rm B}T_\ell}/\mathcal{Z}, \tag{3.7}$$

where $H^{(\rm el)ph}_\ell$, $N_\ell = \sum_q c^\dagger_{\ell q} c_{\ell q}$ and T_ℓ denote the electronic (phononic) Hamiltonians, the numbers of electrons, and the temperatures in leads $\ell = {\rm L}$ and ${\rm R}$, respectively; and $k_{\rm B}$ is the Boltzmann constant, $\mathcal{Z}$ is the partition function.

We invoke a non-equilibrium situation via a temperature modulation on $T_\ell(t)$ in the leads. This can be realized experimentally, for example, by use of a heating/cooling circulator [74]. When a metallic system is heated by a laser beam, the electrons undergo a rather fast thermalization [75–78]. The corresponding relaxation times stem from electron-electron and electron-phonon interactions. For a typical metal, they are of the order of a few femtoseconds or picoseconds, respectively [79, 80].

Throughout the following sections, we assume that the temperature modulations are always sufficiently slow so that the changes of the lead temperatures occur on a time scale much larger than all the thermal relaxation timescales, i.e., $2\pi/\Omega \gg 1\,$ps, where Ω is the driving (angular) frequency. With such adiabatic temperature modulations, the expectation values of the electron and phonon lead operators then read as

$$\langle c^\dagger_{\ell' q'} c_{\ell q}\rangle = f_\ell\left(\varepsilon_{\ell q}, T_\ell(t)\right)\delta_{\ell\ell'}\delta_{qq'} \; , \tag{3.8}$$

$$\langle a^\dagger_{\ell' k'} a_{\ell k}\rangle = n_\ell(\omega_{\ell k}, T_\ell(t))\delta_{\ell\ell'}\delta_{kk'}, \tag{3.9}$$

where

$$f_\ell(\varepsilon_{\ell q}, T_\ell(t)) = \frac{1}{\exp[(\varepsilon_{\ell q} - \mu_l)/k_{\rm B}T_\ell(t)] + 1} \tag{3.10}$$

and

$$n_\ell(\omega_{\ell k}, T_\ell(t)) = \frac{1}{\exp[\hbar\omega_{\ell k}/k_{\rm B}T_\ell(t)] - 1} \tag{3.11}$$

denote the Fermi-Dirac distribution and the Bose-Einstein distribution, respectively, which both inherit a time-dependence due to a temperature modulation.

3.2. Temperature modulation protocols

A Brownian motor is a device that can transport particles within a nonequilibrium, dissipative environment without biased force. Its working principle relies on a symmetry breaking mechanism. This symmetry breaking results from an

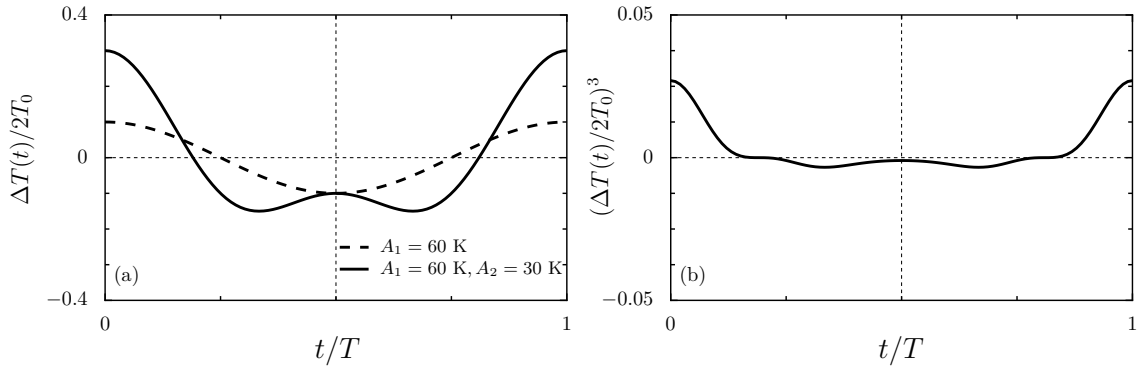

Figure 3.2.: Modulating the lead temperature. (a) The temperature bias $\Delta T(t) \equiv T_L(t) - T_R(t)$ is depicted over a full driving period without and with a second harmonic driving term. The driving amplitude $A_1 = 60$ K is chosen for both cases. (b) Third moment of the signal of the harmonic mixing, $(\Delta T(t)/2T_0)^3$.

asymmetric spatial potential and a temporal modulation of the potential height [64]. Using the same idea, we could design a Brownian heat engine where temperature modulation protocols generate the ratchet heat current and, most importantly, control the heat flow. Two useful time-periodic modulation protocols are: (i) driving only one lead using one harmonic; (ii) driving both leads using a mixing of two harmonics. In both cases, the net thermal bias vanishes on average over a driving period [P1].

3.2.1. Driving one lead only

In case (i), the temperature of one lead is modulated harmonically, while the temperature of the other lead is kept constant, i.e.,

$$\begin{aligned} T_{\mathrm{L}}(t) &= T_0 + A_1 \cos(\Omega t) \ , \\ T_{\mathrm{R}}(t) &= T_0 \ , \end{aligned} \tag{3.12}$$

where A_1 is the driving amplitude, while T_0 is the reference temperature. The driving amplitude A_1 is positive and bounded as $A_1 < T_0$ since $T_{\mathrm{L}}(t)$ has to remain positive at all times.

The temperature difference between the left and right lead is then given by

$$\Delta T(t) = A_1 \cos(\Omega t) \ , \tag{3.13}$$

which is depicted by the dashed curve in Figure 3.2(a) in units of $2T_0$. The net thermal bias vanishes on time average, $\overline{\Delta T(t)} = 0$. Moreover, averaged over one

driving period, the temperatures in both leads are equal to the reference temperature,

$$\overline{T_{\mathrm{L}}(t)} = \overline{T_{\mathrm{R}}(t)} = T_0. \tag{3.14}$$

3.2.2. Driving both leads

In case (ii), we consider temperature modulations applied to both leads in the absence of a thermal bias. The temperature driving consists of a contribution with frequency Ω and a second harmonic with frequency 2Ω. This entails a dynamical symmetry breaking, namely, harmonic mixing [69–73]. The time-dependent lead temperatures are given by

$$T_{\mathrm{L,R}} = T_0 \pm \left[A_1 \cos(\Omega t) + A_2 \cos(2\Omega t + \varphi)\right] , \tag{3.15}$$

so that again

$$\overline{T_{\mathrm{L}}(t)} = \overline{T_{\mathrm{R}}(t)} = T_0 \tag{3.16}$$

and

$$\Delta T(t) = 2[A_1 \cos(\Omega t) + A_2 \cos(2\Omega t + \varphi)] . \tag{3.17}$$

The quantity $\Delta T(t)/2T_0$ is depicted over one period by the solid curve in Figure 3.2(a). Note that, in contrast to the unbiased first moment, the average of the odd third moment over one period does not vanish, which is depicted in Figure 3.2(b). The average temperature bias vanishes irrespective of the phase lag φ.

3.3. Time-averaged driven current

If the lead temperatures are modulated slowly enough ("adiabatic temperature rocking"), the dynamical thermal bias $\Delta T(t)$ can be considered as a static bias at time t in the adiabatic limit $\Omega \to 0$. Thus, both the asymptotic electron and phonon heat currents $J_Q^{\mathrm{el(ph)}}(t)$ can be expressed by Landauer-type formulae for electron heat flux [28, 81] and for the phonon heat flux [36, 38, 82, 83],

$$J_Q^{\mathrm{el}}(t) = \frac{1}{2\pi\hbar} \int_{-\infty}^{\infty} dE E \mathcal{T}^{\mathrm{el}}(E) \left[f(E, T_{\mathrm{L}}(t)) - f(E, T_{\mathrm{R}}(t))\right] , \tag{3.18}$$

$$J_Q^{\mathrm{ph}}(t) = \int_0^{\infty} \frac{d\omega}{2\pi} \hbar\omega \mathcal{T}^{\mathrm{ph}}(\omega) \left[n(\omega, T_{\mathrm{L}}(t)) - n(\omega, T_{\mathrm{R}}(t))\right] , \tag{3.19}$$

where electrons with energy E and phonons with frequency ω are scattered from left to right lead, respectively. Following the argumentation of Section 2.2, we count the energy starting from the chemical potential μ, such that the energy E

carried by each electron is actually the carried heat excluding the part embodied by the chemical potential.

We have already derived Eq. (3.18) in Section 2.3, see Eq. (2.41). This expression is actually the Seebeck current generated by static thermal bias. Here, $\mathcal{T}^{\rm el}(E)$ denotes the temperature independent transmission coefficients for electrons which assumes a Breit-Wigner form (see also Eq. (2.40)),

$$\mathcal{T}^{\rm el}(E) = \frac{\Gamma^2}{(E-\varepsilon_0)^2+\Gamma^2}\,, \tag{3.20}$$

where we have assumed symmetric electron wire-lead coupling, i.e., $\Gamma_{\rm L} = \Gamma_{\rm R} = \Gamma$.

The phonon transmission coefficient $\mathcal{T}^{\rm ph}(\omega)$ is evaluated following Ref. [38]. As shown in Appendix B, it assumes a Breit-Wigner form for one phonon mode as well, i.e., the temperature-independent phonon transmission probability reads

$$\mathcal{T}^{\rm ph}(\omega) = \frac{4\omega^2\gamma^2(\omega)}{(\omega^2-\omega_0^2)^2+4\omega^2\gamma^2(\omega)}\,, \tag{3.21}$$

where $\gamma(\omega) = ae^{-\omega/\omega_{\rm D}}$ characterizes the coupling between the central phononic mode and the phonon modes in the leads. Here $\omega_{\rm D}$ is the Debye cut-off frequency of phonon reservoirs in the lead and $a = \pi g^2/4mM\omega_{\rm D}^3$ incorporates the symmetric phonon wire-lead coupling $g = g_{\rm L} = g_{\rm R}$.

Since there is no electron-phonon interaction, the time-dependent, asymptotic total heat current is the sum of the electronic and phononic heat currents,

$$J_Q(t) = J_Q^{\rm el}(t) + J_Q^{\rm ph}(t)\,. \tag{3.22}$$

It inherits the periodicity $2\pi/\Omega$ of the external driving field from the distributions (see Eqs. (3.18) and (3.19)),

$$J_Q(t) = J_Q(t+2\pi/\Omega). \tag{3.23}$$

We henceforth focus on the stationary heat current $\overline{J_Q}$ which follows from the average over a full driving period:

$$\overline{J_Q} = \frac{\Omega}{2\pi}\int_0^{2\pi/\Omega} J_Q(t)dt. \tag{3.24}$$

3.4. Numerical parameters

In our numerical investigations, we employ the electron wire-lead tunnel rate $\Gamma = 0.11\,\text{eV}$, which has also been used to describe electron tunneling between

a phenyldithiol (PDT) molecule and gold contact [34]. The phonon frequency $\omega_0 = 1.4 \times 10^{14}\,\mathrm{s}^{-1}$ is typical for a carbon-carbon bond [84]. For the Debye cut-off frequency for phonon reservoirs we use the value for gold, which is $\omega_\mathrm{D} = 2.16 \times 10^{13}\,\mathrm{s}^{-1}$. The phonon coupling frequency $a = 1.04 \times 10^{15}\,\mathrm{s}^{-1}$ is chosen such that the static thermal conductance assumes the value $50\,\mathrm{pWK}^{-1}$ which has been measured in experiments with alkane MJs [85].

These parameters imply physical time scales which are worth being discussed. During the dephasing time, electron-phonon interactions within the wire destroy the electron's quantum mechanical phase. If this time is larger than the dwell time, i.e., the time an electron spends in the wire, the electron transport is predominantly coherent [35]. Following Ref. [35], we estimate the dwell time by the tunneling traversal time

$$\tau \sim \frac{\hbar}{\sqrt{\varepsilon_0^2 + \Gamma^2}} \tag{3.25}$$

which for our parameters is of the order $\tau \sim 5\,\mathrm{fs}$ and, thus, much shorter than the typical electron-phonon relaxation time (dephasing time) which is of order of 1 ps. This implies that the electronic motion is predominantly coherent, so that the electron-phonon interaction within the wire can be ignored. The phonon relaxation time within the wire can be estimated as $1/a \sim 1\,\mathrm{fs}$. Among the above mentioned time scales, the slowest one is that of the electron-phonon relaxation, which is of the order of $1\,\mathrm{ps}$. Thus, the regime of validity of our assumption for adiabatic temperature modulations is justified when the driving frequency is much slower the electron-phonon relaxation rate within lead, i.e., $\Omega \ll 1\,\mathrm{THz}$.

In fact, as far as the adiabatic condition is satisfied, the heat current does not depend on the driving frequency. This can also be shown mathematically. Together with Eq. (3.12), Eq. (3.24) can be rewritten as

$$\overline{J_Q} = \frac{\Omega}{2\pi} \int_0^{2\pi/\Omega} J_Q(\Omega t) dt. \tag{3.26}$$

Replacing the independent variable in the above integral as $\Omega t \to \tau$ and changing the integration limits accordingly, we obtain

$$\overline{J_Q} = \frac{1}{2\pi} \int_0^{2\pi} J_Q(\tau) d\tau. \tag{3.27}$$

This integral does not depend on the driving frequency any more and the integration interval ranges from 0 to 2π. Thus, the modulation is not bound to a certain frequency. However the adiabatic condition should be fulfilled, i.e., the driving frequency always needs to be smaller than all the relaxation and tunneling rates in the whole system.

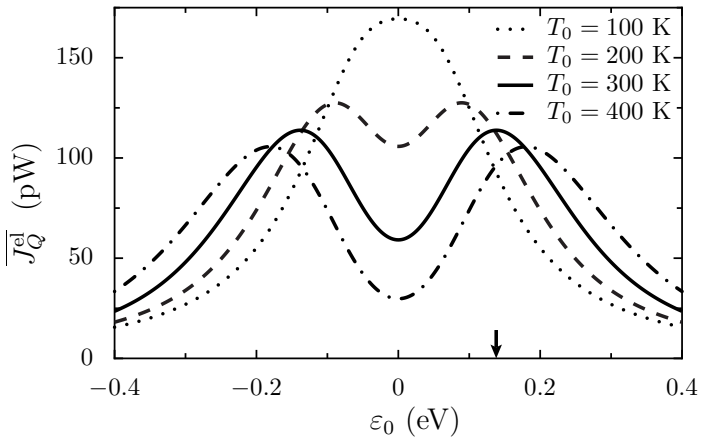

Figure 3.3.: Directed electronic heat current $\overline{J_Q^{\rm el}}$ as a function of on-site energy ε_0 for different reference temperatures T_0 and temperature oscillation amplitude $A_1 = 30$ K ($A_2 = 0$). The arrow marks the on-site energy $\varepsilon_0 = 0.138$ eV for which the pumped electron current assumes at temperature $T_0 = 300$ K its maximum. The adiabatic rocking frequency is $\Omega = 3.92$ GHz. All the other parameters can be found in Section 3.4.

3.5. Results and discussion

3.5.1. Driving one lead only

In what follows, unless mentioned explicitly, we assume unbiased source-drain leads with chemical potentials $\mu_{\rm L} = \mu_{\rm R} = \mu$, i.e., there is no voltage bias acting.

Both the electronic and the phononic heat currents averaged over one driving period are obtained by numerically evaluating the integrals in Eqs. (3.24), (3.18), and (3.19). As expected for an adiabatic theory, we observe that the average heat current $\overline{J_Q}$ is independent of the driving frequency Ω. This is in accordance with the findings for ballistic heat transfer in the adiabatic regime.

Heat current sensitive to on-site energy

In an experiment, the molecular level ε_0 can be manipulated by a gate voltage, which influences only the electrons. This allows one to tune the electron transport while keeping the phonons untouched. In Figure 3.3, we depict the net electron heat current $\overline{J_Q^{\rm el}}$ as a function of ε_0 for a fixed driving amplitude. We find that the heat current possesses an extremum for $\varepsilon_0 = 0$, i.e., when the on-site energy is aligned with the Fermi energy. Interestingly enough, this extremum is a maximum for low reference temperature T_0 and turns into a local minimum

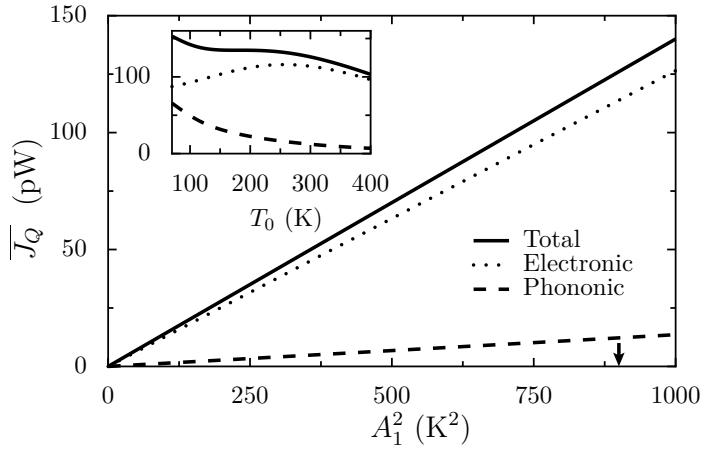

Figure 3.4.: Total electronic and phononic time-averaged, directed heat current $\overline{J_Q}$ as a function of the squared driving amplitude A_1^2 with reference temperature at $T_0 = 300\,\mathrm{K}$ for the on-site energy $\varepsilon_0 = 0.138\,\mathrm{eV}$. The dotted line represents the electronic contribution; the dashed line represents the phononic one. The inset depicts the directed heat current as a function of the reference temperature T_0 for the amplitude $A_1 = 30\,\mathrm{K}$ ($A_2 = 0$) marked by the arrow in the main panel. All the other parameters can be found in Section 3.4.

when the temperature exceeds a certain value. This implies that the net electron heat current is rather sensitive to the difference between the on-site energy and the Fermi energy. This property thus provides an efficient way to determine experimentally the Fermi energy of the wire as an alternative to, e.g., measuring the thermopower as proposed in Ref. [34]. For large gate variations we find that the directed electron heat current is significantly suppressed since the wire level is far off the electron thermal energy, i.e., $\varepsilon_0 \gg k_\mathrm{B} T_0$. The directed heat current then is dominated by the phonon heat flux. As temperature is increased, the peak positions of the pumped electron heat current shift outwards, away from the Fermi energy. At room temperature $T = 300\,\mathrm{K}$, the peak positions are located at $\varepsilon_0 = \pm\, 0.138\,\mathrm{eV}$.

Scaling behavior for small driving strengths

Figure 3.4 shows the total heat current $\overline{J_Q}$ as a function of the driving amplitude A_1 for the reference temperature $T_0 = 300\,\mathrm{K}$ and the electronic site above the Fermi level. For weak driving ($A_1 \ll T_0$), we find

$$\overline{J_Q^{\mathrm{el(ph)}}} \propto A_1^2 \tag{3.28}$$

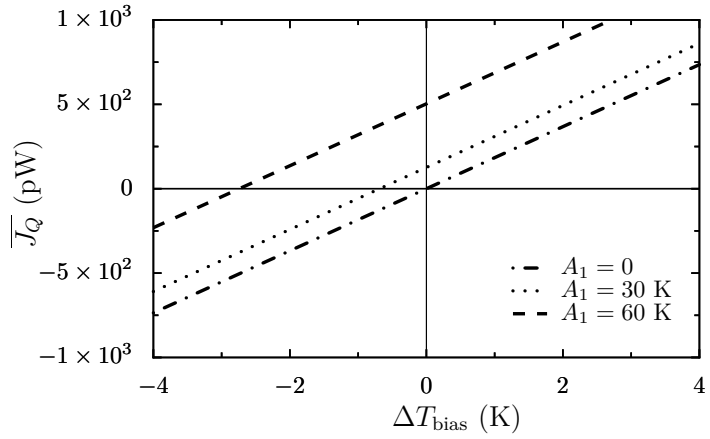

Figure 3.5.: Total directed heat current $\overline{J_Q}$ as a function of static thermal bias $\Delta T_{\rm bias}$ for different driving amplitude strengths A_1 for an adiabatic temperature modulation, with $A_2 = 0$. The reference temperature is set as $T_0 = 300$ K and the electronic wire level is set as $\varepsilon_0 = 0.138$ eV. All the other parameters can be found in Section 3.4.

for both the electronic and the phononic contribution. This behavior can be understood from a Taylor expansion of the Fermi-Dirac distribution f and the Bose-Einstein distribution n,

$$\begin{aligned}\mathcal{D}(\xi, T_{\rm L}) - \mathcal{D}(\xi, T_0) &= \mathcal{D}(\xi, T_0 + \Delta T) - \mathcal{D}(\xi, T_0) \\ &= \mathcal{D}'(\xi, T_0)\Delta T(t) + \frac{\mathcal{D}''(\xi, T_0)}{2}[\Delta T(t)]^2 + \cdots ,\end{aligned} \tag{3.29}$$

where $\mathcal{D} = f, n$ represents either distribution, while $\mathcal{D}'$ and $\mathcal{D}''$ denote derivatives with respect to temperature difference. Note that the time dependence stems solely from the temperature difference $\Delta T(t)$. After a cycle average over the driving period, the first term in the expansion vanishes owing to $\overline{\Delta T(t)} = 0$. Therefore, the leading term of the heat current is of second order, i.e., $\propto \overline{[\Delta T(t)]^2}$, which yields

$$\overline{J_Q^{\rm el(ph)}} \propto \int_0^{2\pi/\Omega} [\Delta T(t)]^2 dt \propto A_1^2, \tag{3.30}$$

as observed numerically. We also plot the directed heat current as a function of the reference temperature T_0 in the inset of Figure 3.4. Upon increasing the reference temperature, the directed phonon heat current decreases monotonically. However, the emerging total heat current exhibits a relatively flat behavior in a large temperature range. This is due to the combined effect from phonons and electrons. At high temperatures, the electron contribution dominates the directed heat flow.

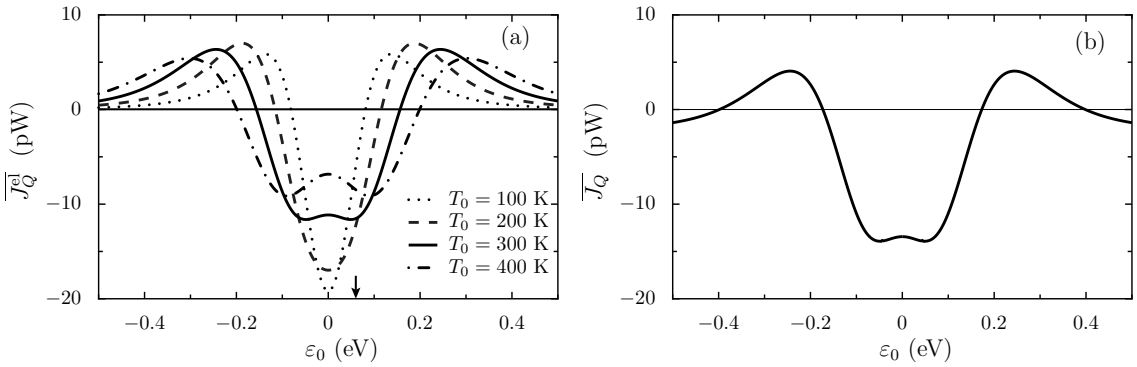

Figure 3.6.: (a) Directed electron heat current $\overline{J_Q^{\rm el}}$ as a function of the wire level ε_0 for various reference temperatures T_0. The driving parameters are $A_1 = A_2 = 30$ K and $\varphi = 0$. (b) Total net heat current $\overline{J_Q}$ as function of the wire level ε_0 for reference temperature $T_0 = 300$ K and amplitudes $A_1 = A_2 = 30$ K, with harmonic mixing phase lag $\varphi = 0$. All the other parameters can be found in Section 3.4.

Thermal load characteristics

Thus far, we have studied heat pumping in the absence of any constant temperature bias, i.e., for $\overline{\Delta T(t)} = 0$. We next introduce a static thermal bias such that a thermal bias $\Delta T_{\rm bias} := \overline{\Delta T(t)} \neq 0$ emerges. The resulting total directed heat current $\overline{J_Q}$ is depicted in Figure 3.5. Within this load curve, we spot a regime with negative static thermal bias $\Delta T_{\rm bias} < 0$ and positive-valued overall heat flow until $\Delta T_{\rm bias}$ reaches the stop-bias value, i.e., we find a so-called Brownian heat-ratchet effect [16, P1]. This means that heat can be pumped against a thermal bias from cold to hot like in a conventional heat pump. The width of this regime scales with the driving amplitude A_1^2, (cf. Figure 3.5).

3.5.2. Driving both leads

In Figure 3.6(a), we depict the resulting electron heat current $\overline{J_Q^{\rm el}}$ as a function of the on-site energy ε_0 for various reference temperatures T_0. At low temperatures, the net electron heat current exhibits a local minimum at the Fermi energy. With increasing reference temperature T_0, this minimum then develops into a local maximum with two local minima in its vicinity. The arrow in Figure 3.6(a) marks the minimum at $\varepsilon_0 = 0.049$ eV for $T_0 = 300$ K. It is interesting that the direction of the net electron heat current can be controlled by the gate voltage. For an electron wire level close to the Fermi level, the directed electron heat current is negative. Upon tuning the gate voltage, the heat current undergoes a reversal and becomes

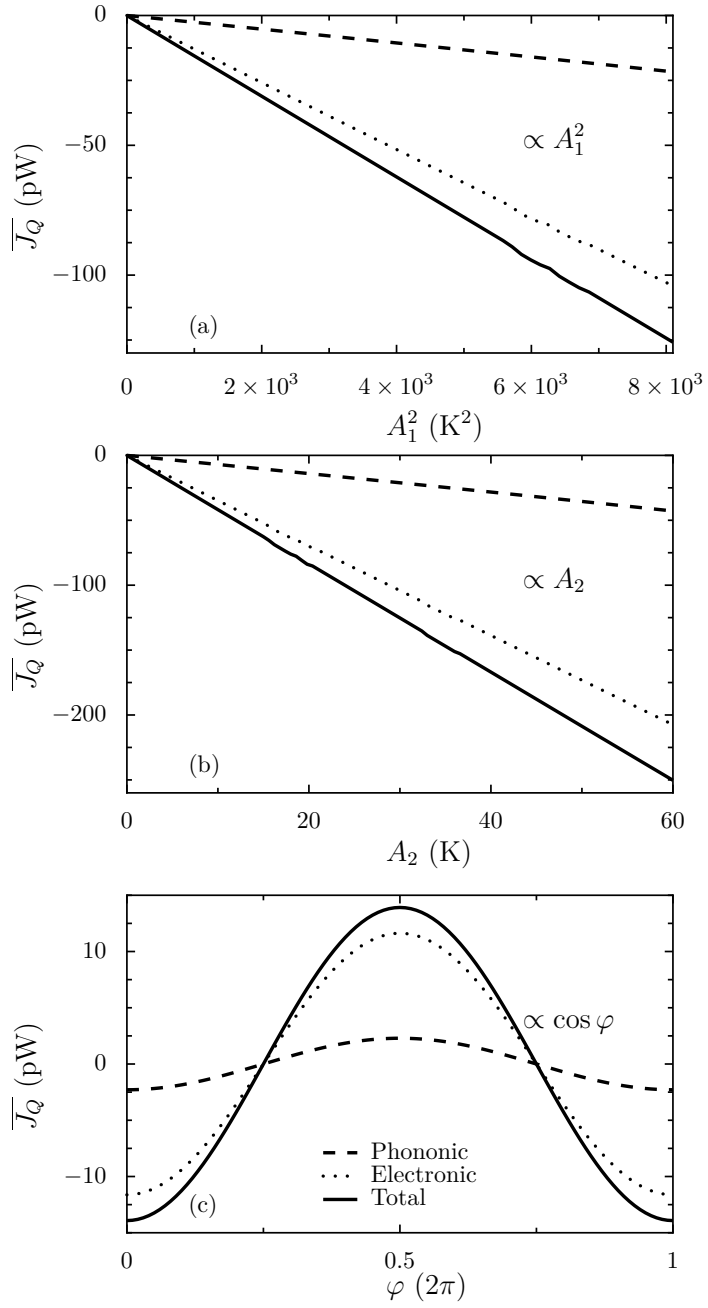

Figure 3.7.: Heat current $\overline{J_Q}$ as a function of (a) the fundamental driving strength A_1, where $A_2 = 30\,\mathrm{K}$ and $\varphi = 0$ and (b) the second-harmonic amplitude A_2, where $A_1 = 90$ K and $\varphi = 0$. (c) Dependence of $\overline{J_Q}$ on the relative phase φ for $A_1 = A_2 = 30$ K. The reference temperature is $T_0 = 300\,\mathrm{K}$, while the wire level is $\varepsilon_0 = 0.049\,\mathrm{eV}$. All the other parameters can be found in Section 3.4.

positive when ε_0 is larger than $0.15\,\mathrm{eV}$ (at reference temperature $T_0 = 300\,\mathrm{K}$) and eventually approaches zero again for large detuning.

Figure 3.6(b) shows the corresponding sum of electron and phonon heat flows, i.e., the net heat current $\overline{J_Q}$ as a function of wire level ε_0. The net phonon heat current $\overline{J_Q^{\mathrm{ph}}}$ is negative for these parameters (not depicted) and is not sensitive to the gate voltage. As a consequence, this sum of phonon and electron heat transport, $\overline{J_Q}$, exhibits *multiple current reversals* as the on-site energy ε_0 increases. For small values of ε_0, i.e., close to the Fermi surface, both the electron and the phonon heat fluxes are negative and in phase with the driving and the absolute value of the total heat current assumes its maximum (at which the heat current is negative). For intermediate values of ε_0, the direction of total net current $\overline{J_Q}$ is reversed due to the dominating positive contribution of the electrons. At even larger values of ε_0, the electron heat current almost vanishes, so that the total heat current is dominated by the negative-valued contribution of the phonons. In the limit of large ε_0, we find saturation at a negative value.

In Figure 3.7, we also study the net electron and phonon heat currents as functions of the driving amplitudes A_1, A_2 and the relative phase φ. Both current contributions scale as

$$\overline{J_Q^{\mathrm{el/ph}}} \propto A_1^2 A_2 \cos(\varphi), \tag{3.31}$$

which implies that they can be manipulated simultaneously. This behavior can be understood by again expanding the Fermi-Dirac distribution f and the Bose-Einstein distribution n in ΔT around the average temperature T_0,

$$\begin{aligned} \mathcal{D}(\xi, T_{\mathrm{L}}) - \mathcal{D}(\xi, T_{\mathrm{R}}) &= \mathcal{D}(\xi, T_0 + \Delta T/2) - \mathcal{D}(\xi, T_0 - \Delta T/2) \\ &= \mathcal{D}'(\xi, T_0)\Delta T(t) + \frac{\mathcal{D}'''(\xi, T_0)}{24}[\Delta T(t)]^3 + \cdots , \end{aligned} \tag{3.32}$$

where $\mathcal{D} = f, n$ represents the distribution function of electrons and phonons, respectively. The terms of even order in ΔT vanish owing to the anti-symmetric temperature modulation. Thus, the heat currents are governed by the time average of the odd powers $[\Delta T(t)]^{2n+1}$ with $n > 1$, since $\overline{\Delta T} = 0$. It can be easily verified that all these time-averaged odd moments vanish if either amplitude, A_1 or A_2 vanishes. Note that the lowest-order contribution, i.e., the third moment, reads as

$$\overline{[\Delta T(t)]^3} = 8 A_1^2 A_2 \cos(\varphi)\ . \tag{3.33}$$

In Figure 3.2(b) the quantity $(\Delta T(t)/2T_0)^3$ is depicted over one period. Thus, for small driving amplitudes, $A_1, A_2 \ll T_0$, the net electron and phonon heat current are expected to be proportional to $A_1^2 A_2 \cos\varphi$ as corroborated with the numerical results depicted in Figs. 3.7(a,b,c). This proportionality to $\cos\varphi$, see Figure 3.7(c), is even more robust than expected a priori; this is so because the averaged 5-th and 7-th moment are proportional to $\cos(\varphi)$, as well, i.e., $\overline{[\Delta T(t)]^5}, \overline{[\Delta T(t)]^7} \propto$

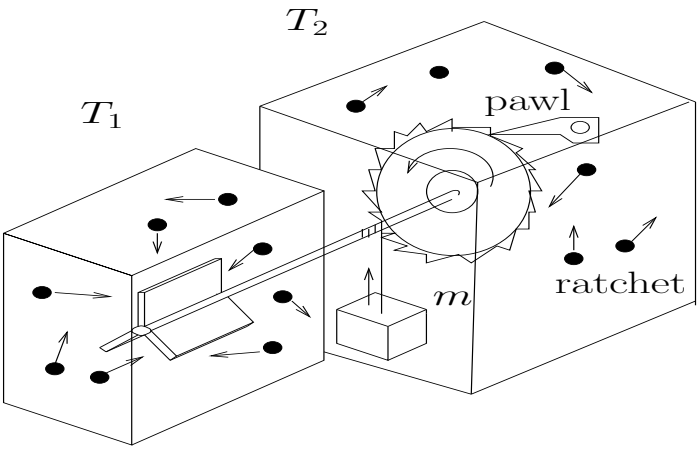

Figure 3.8.: Schematic graph for the ratchet and pawl setup. This setup is composed of an axle with one paddle attached on the left hand side and a ratchet on the right hand side. Both ends are situated inside boxes that are filled with gases in equilibrium at temperatures T_1 and T_2. Due to the asymmetry of the ratchet, the pawl allows the ratchet to rotate in one direction only but prevents it from rotating in the other direction. Furthermore, a weight m can be added to the axle.

$\cos(\varphi)$. This behavior can be employed for a sensitive control of the heat current: The direction of the heat current can be reversed by merely adjusting the relative phase φ between the two harmonics. Note that for the parameters used in the figure, the net electron heat current $\overline{J_Q^{\mathrm{el}}}$ exceeds the net phonon heat current $\overline{J_Q^{\mathrm{ph}}}$ roughly by a factor of five.

3.6. Origin of the quantum heat ratchet

In the above sections, we have found nonzero average heat currents across a quantum MJ with specific adiabatic temperature modulations either in one lead only or in both leads. This concept of heat transport does not require any net thermal bias, i.e., we have effectively proposed a setup for a quantum heat ratchet.

This idea of a quantum heat ratchet originates from the field of Brownian motors, which relies on the ratchet effect. A ratchet and pawl setup, depicted in Figure 3.8, was first analyzed in the year 1912 by the Polish physicist Marian Smoluchowski. About half a century later, in 1962, Richard Feynman took this setup on his lectures and made it famous. The paddle in the left box is responsible for the Brownian motion, while the ratchet-pawl setup controls its rotation direction. Now the question could be asked whether one can extract useful work

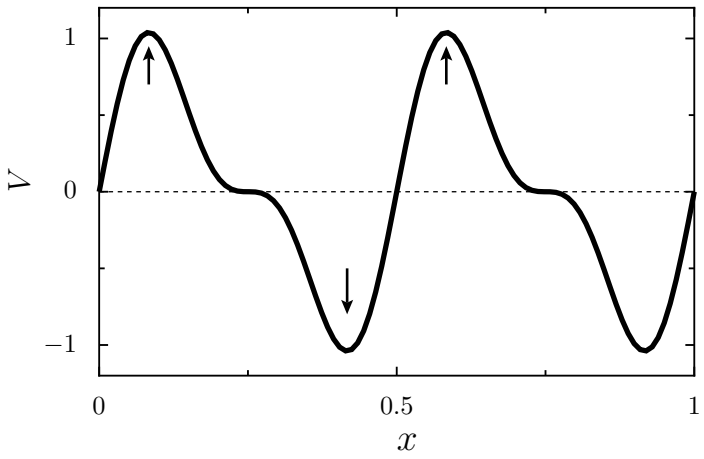

Figure 3.9.: Asymmetric and periodic potential. The middle arrow denotes the initial position of the particles. The left and right arrows denote positions of its adjacent potential maxima.

from this setup and lift the weight with mass m if $T_1 = T_2$. If so, the second law of thermodynamics would be violated. Smoluchowski, however, pointed out that this is impossible. The key point is that the pawl is also subjected to Brownian motion. Therefore, it possibly does not always work in the way it would need to. Hence the only possible way in which one can extract work is to set the setup in nonequilibrium, where the second law makes no assertion.

The question of how to extract useful work from a fluctuating environment and how to allow motion of particles is in the focus of research on Brownian motors, from where we adopt our idea for a quantum heat ratchet. We take one proposal of the Brownian motor as an example. Suppose that we have a periodic potential, as depicted in Figure 3.9, composed of two harmonics (for details see Ref. [65]). The depth of the potential is larger than the thermal noise strength $k_{\mathrm{B}}T$, where T is the temperature of the surrounding. The noninteracting particles, which are initially located in the vicinity of a potential minimum (as denoted by the middle arrow), are in a viscous environment.

One potential well, being the repeated units of the periodic potential, has two unequal slopes. In the proposal of the Brownian motor, the potential is turned on and off repeatedly. When the potential is turned off (depicted by the dashed curve), the particles are only subjected to the Brownian motion enforced by the viscous surrounding. The probability that they pass the position of the right adjacent potential maximum (denoted by the right arrow) is larger than the probability that they pass the left one (denoted by the left arrow), because the right one is closer. When the potential is turned on again, more particles will slip to the right adjacent potential minimum, because now the motion of the particles is

dominated by the potential. In this way, a net current to the right emerges [65].

Quantum ratchet could also be designed and realized when the particle obeys the law of quantum mechanics. Apart from the motion described above, the tunneling effect, which occurs only in quantum mechanics, plays an important role. A current reversal has been predicted theoretically [71, 86] and observed experimentally [87] when temperature is lowered to a critical point where quantum mechanics starts to work. A paper on transport quality of the quantum ratchet has been published in Ref. [P4].

Some necessary conditions to realize the Brownian motor can be concluded from this example. First, as suggested by its name, particles should be subjected to Brownian motion in a viscous environment. Second, we need energy input, ensuring that energy is conserved in the process. In the above example, the energy input happens via modulating the height (or depth) of the potential well. Last but not least, symmetry of the system should be broken. This is automatically provided by the asymmetry of the potential, implying that the particles diffuse to the nearby minima with different probabilities when the potential is turned off.

The condition of symmetry breaking is essentially important in the frame of this work. From Eqs. (3.18), (3.19) and (3.24), one possible symmetry in the system is given by

$$J_Q(t) = -J_Q(\pi/\Omega - t) \; . \tag{3.34}$$

If this symmetry is not violated, nonzero average heat current does not occur.

For the temperature difference of case (ii), where we modulate the temperatures in both leads, we have $\Delta T(t) \neq -\Delta T(\pi/\Omega - t)$ (see solid curve in Figure 3.2(a)). Then the symmetry condition (3.34) is violated as indicated by the Landauer-type formulae, Eqs. (3.18) and (3.19), and we have nonzero average heat current. For case (i), where we modulate the temperature only in the left lead, we have $\Delta T(t) = -\Delta T(\pi/\Omega - t)$ (see dashed curve in Figure 3.2(a)) then symmetry should not be broken from a naive point of view. Nonetheless, for the distribution differences in Eqs. (3.18) and (3.19), we find

$$\mathcal{D}_{\rm L}(T_0 + \Delta T) - \mathcal{D}_{\rm R}(T_0) \neq -[\mathcal{D}_{\rm L}(T_0 - \Delta T) - \mathcal{D}_{\rm R}(T_0)], \tag{3.35}$$

where $\Delta T = A_1 \cos(\Omega t)$. This inequality stems from the fact that the distribution functions are strongly nonlinear functions of the temperature T, see Eqs. (3.10) and (3.11). The differences of the distributions on both sides of Eq. (3.35) do not depend the temperature difference linearly, as indicated in Eq. (3.29). Thus the symmetry condition (3.34) is also broken for case (i). Moreover, the linear terms of the differences vanish after averaging over one driving period, whereas the higher moments do not. This is the essential reason why both of our quantum heat ratchets work.

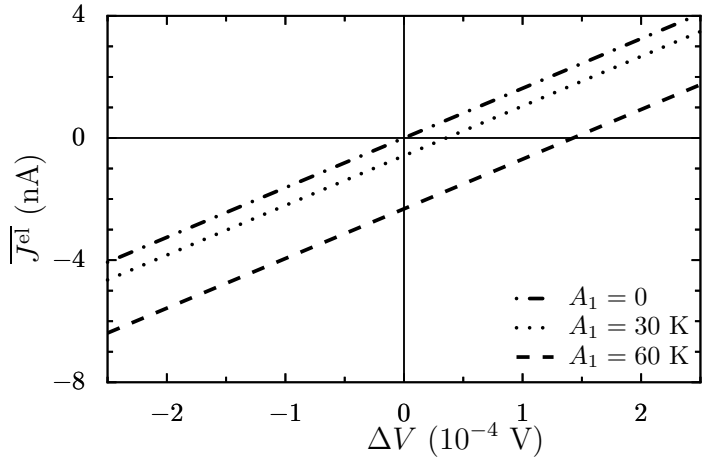

Figure 3.10.: The time-averaged directed electric current $\overline{J^{\rm el}}$ as function of the static voltage bias ΔV for different temperature amplitudes A_1, with $A_2 = 0$. The reference temperature is $T_0 = 300\,\mathrm{K}$ and the electronic wire level is at $\varepsilon_0 = 0.138\,\mathrm{eV}$. All the other parameters can be found in Section 3.4.

3.7. Ratchet "Seebeck" effect

In 1821, the German physicist Thomas Johann Seebeck found that a compass needle was deflected when two metal wires were connected at its two ends with the two junctions being at different temperatures. In addition a current was generated in the circuit. This phenomenon of a temperature difference generating a voltage is named after him as Seebeck effect, while the Peltier effect does the opposite thing.

The Seebeck effect is described by the thermopower (Seebeck coefficient), which is defined as

$$\mathcal{S} = -\lim_{\Delta T \to 0} \frac{\Delta V}{\Delta T}, \tag{3.36}$$

where ΔT is the temperature difference ΔV the voltage generated. The sign of $\mathcal{S}$ can tell whether a net of positive or negative charge carriers builds up the voltage bias. From the above definition, the Seebeck coefficient has the dimension $\mathrm{V/K}$. The most efficient materials obtained so far have hundreds of $\mu\mathrm{V/K}$ [88].

As can be deduced from Figure 3.5, a zero-biased temperature modulation generates a finite net heat flow similar to the heat flow that would be induced by a static thermal bias. Near equilibrium, i.e., within the linear response regime, Onsager symmetry relations for conjugated transport quantities are expected to hold. Therefore, the adiabatic temperature modulations are expected to induce an *electric current* as well. This net adiabatic electric pump current can be obtained

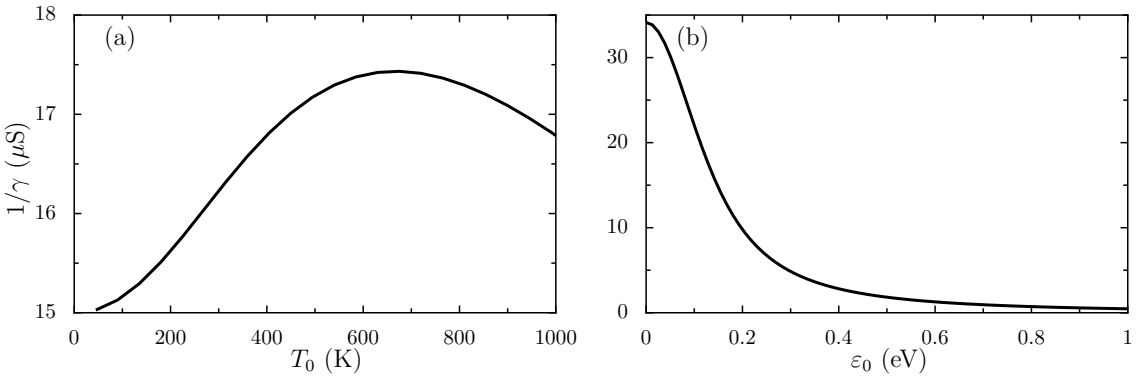

Figure 3.11.: The reciprocal of the quantity γ as a function of (a) the reference temperature T_0 with $\varepsilon_0 = 0.138$ eV and (b) the on-site energy ε_0 with $T_0 = 300$ K. For both cases, the driving amplitude is set as $A_1 = 30$ K, with $A_2 = 0$. All the other parameters can be found in Section 3.4.

by means of the period-averaged Landauer expression which explicitly reads as

$$\overline{J^{\mathrm{el}}} = \frac{\Omega}{2\pi}\int_0^{2\pi/\Omega} dt \frac{e}{h}\int dE\, \mathcal{T}(E)\left[f_{\mathrm{L}}(E,T_{\mathrm{L}}) - f_{\mathrm{R}}(E,T_{\mathrm{R}})\right] \ . \tag{3.37}$$

In addition, we add a net static voltage bias ΔV. Figure 3.10 depicts the net electric current-voltage characteristics $\overline{J^{\mathrm{el}}}(\Delta V)$ in the presence of an unbiased temperature modulation while importantly no external thermal bias is applied. For a positive bias voltage $\Delta V > 0$, the net electric current is negative, i.e., the system effectively acts as an "electron pump".

When the voltage bias ΔV assumes a certain value, namely, the so called stop voltage ΔV_{stop} , the bias-induced current and the driving-induced current compensate each other. The value can be interpreted as a sole heat-ratchet induced thermopower. We term this phenomenon *ratchet Seebeck effect*. Knowingly, the usual thermopower (Seebeck coefficient), see Eq. (3.36), is defined by means of the change in induced voltage per unit change in applied temperature bias under conditions of zero electric current [89]. Here, in the absence of a net thermal bias, we introduce instead the quantity $\gamma = |\Delta V_{\mathrm{eff}}/\overline{J^{\mathrm{el}}(\Delta V = 0)}|$, where ΔV_{eff} denotes the effective static voltage bias which yields the *identical* electric heat current $\overline{J^{\mathrm{el}}(\Delta V = 0)}$ as generated by our imposed temperature modulation. We find this effective voltage bias precisely matches the above mentioned stop-voltage, i.e., $\Delta V_{\mathrm{eff}} = -\Delta V_{\mathrm{stop}}$. Due to the linear $\overline{J^{\mathrm{el}}}$–$\Delta V$ characteristics, as evidenced with Figure 3.10, the quantity γ is independent of the amplitude of the temperature modulation. In Figures 3.11(a) and 3.11(b), we depict the reciprocal of γ as a function of reference temperature T_0 [Figure 3.11(a)] and on-site energy ε_0 [Figure 3.11(b)], respectively. We find a resonance like dependence $1/\gamma$ as a function

of the reference temperature T_0, while it decreases monotonically with increasing on-site energy ε_0. Note also that this quantity γ is a symmetric function of ε_0.

One possible application of the ratchet Seebeck effect is the generation of electricity in a situation where the temperature difference is fluctuating with time.

3.8. Summary

We have demonstrated the possibility of steering heat across a gated two-terminal molecular junction, owing to lead temperatures that undergo adiabatic, unbiased, time-periodic modulations. In a realistic molecule, the heat flow is carried by electrons as well as by phonons. Our study considers both contributions. Two scenarios of temperature modulations have been investigated, namely directed heat flow (i) induced by periodic temperature manipulation in one connecting lead only and (ii) created by a temperature modulation that includes a contribution oscillating with twice the fundamental frequency. In both cases, we predict a finite heat current which is related to dynamical breaking of reflection symmetry. A necessary ingredient is the non-linearity of the initial electron and phonon distribution, which is manifest in the Fermi-Dirac distribution and the Bose-Einstein distribution. The first scenario yields sizable heat currents proportional to the squared amplitude of the temperature modulation. The resulting heat flow occurs in the absence of a static thermal bias.

We have also studied heat pumping against an external static thermal bias and computed the corresponding thermal heat-current load characteristics. Moreover, the ratchet heat flow in turn generates also an electric current. This ratchet heat current induces a novel phenomenon, namely a ratchet-induced, effective thermopower, as depicted in Figure 3.10.

When the asymmetry is induced by temperature rocking at both leads, the resulting net heat current becomes smaller in size. This is because the leading-order time-averaged heat flow now starts out with the third moment of the driving amplitude. The benefit of this second scenario is the possibility of controlling efficiently both the magnitude and the sign of the net heat flow. For example, the direction of the heat current can be readily reversed via the gate voltage or the relative phase between two temperature modulations that are harmonically mixed. When adjusting the gate voltage, the directed heat current experiences multiple current reversals. The directed heat flow is even up to 7-th order in the amplitude proportional to the cosine of the phase between the fundamental frequency and the second harmonic. This allows robust control even for relatively large temperature amplitudes.

These theoretical findings may also inspire experimental efforts to steer heat in a controlled manner across a molecular junction as well as the development

of new concepts for measuring system parameters via their impact on the heat current. For example, as elucidated in Section 3.5, the Fermi energy can be sensitively gauged in this way.

4. Summary and Outlook

The control of heat transport in nanoscale systems has become a more and more important issue over the past years. A detailed understanding of the underlying mechanisms is even more important than for macroscopic systems, because the structural stability of any nanoscale system, e.g., a molecular junction, depends sensitively on the heat flux across it. Despite that, this topic has not attracted much attention in the literature so far, the more so as a measurement of heat flow in an experiment is not a straightforward task.

This thesis presents two central aspects about heat transport in molecular junctions, which are elucidated in Chapters 2 and 3, respectively. In Chapter 2, we have considered the electronic heat current across a molecular wire composed of one single energy level. There, temperature difference between both leads has been assumed to be constant. Moreover, we have neglected electron-phonon interactions and electron-electron interactions. Such a simplification can be justified in situations that involve a short wire. There, the Coulomb interaction due to a double occupancy of the wire shifts a second energy level far above the Fermi level so that its role for thermal transport can be neglected. Likewise, the dwell time of an electron is very short as compared with the electron-phonon relaxation time. In contrast to prior works [42,43], however, we take into account the dependence of the transmission coefficient on electron energies. Within Green function approach, we derive an explicit expression for the power spectrum density of the heat current fluctuations. With this result at hand, we explore different regimes of electron transport and demonstrate that the heat noise in fact is quite distinct from its electric counterpart.

As a consequence, we find that the wire-lead coupling strength can change the dependences of power spectral densities on other parameters. At absolute zero temperature, we observe that a power spectral density still depends on frequency and it obeys power laws in different frequency regions. Now, if the wire-lead coupling strength approaches infinity, the dependence of the power spectral density on frequency becomes uniform throughout the whole frequency region, which is in full agreement with the results obtained in Refs. [42,43].

In Chapter 3, we have focused on shuttling heat across a molecular junction with the latter acting as a quantum heat ratchet. Apart from an electronic heat current deduced from the simple, idealized model used in Chapter 2, we have considered a separate, phononic contribution to the heat current, based on a

model given in Ref. [38]. Likewise, we have modeled the vibration of the central molecule in a molecular junction by means of one single phononic mode. With respect to the temperatures of the lead reservoirs, we have considered two different modulation schemes in the absence of a finite net thermal bias. For both the electron and the phonon reservoirs, this temperature modulation was chosen to be adiabatically slow. In a first approach, only the temperature of one lead was modulated via an ac-drive, whereas in the second modulation scheme employed here we have taken into account a modulation of both lead temperatures. In the latter case, the leads are driven with a mutual phase lag and using multiple harmonics of one driving frequency. For both schemes we find that finite average heat currents can be generated. The electronic parts of these heat currents turn out to be very sensitive to the energetic difference between the single energy level of the junction molecule and the chemical potential of both leads. By contrast, the phononic contribution to the heat current is not sensitive to this detail. As a consequence, for the second modulation scheme, the total heat current exhibits multiple current reversals. We also illustrate that a heat current generated by means of those temperature modulations can even persist against a thermal bias. As a result, the second modulation scheme allows for a better control of the heat flow across the molecular junction, especially by tuning the phase lag. Finally, we analyze the ratchet effects that occur because of the mentioned modulations and point out the symmetry breakings that are necessary to obtain a nonzero average heat current.

In an experiment, the concept of a quantum heat ratchet could be realized in a semiconductor heterostructure, with a quantum dot with discrete energy levels playing the role of the molecule in the junction. A corresponding experiment is currently planned in the group of Dr. Stefan Ludwig at Ludwig-Maxmilians-Universität in Munich. The results will hopefully allow us to substantiate the models presented in this thesis. Apart from inspiring experimental efforts to steer heat in a controlled manner across a molecular junction, our theoretical findings could further motivate the development of new concepts for measuring system parameters via their impact on the heat current. For example, the Fermi energy can be sensitively gauged in this way. There is also an intriguing perspective to apply an external periodic perturbation with the goal to control the spectral properties of the heat noise, similar to electronic shot-noise control in ac-driven nanoscale conductors [47]. This idea can be realized, for example, by subjecting the molecular wire to strong laser radiation [48] or by using direct modulations of the gate voltage. We conjecture that the role of laser radiation may give rise to novel phenomena to be explored further by combining a Floquet theory for the driven system with the nonequilibrium Green function formalism [19,39,47].

Finally, a more realistic model of heat transport in real molecular junctions would involve the complexity of electron-electron and electron-phonon interac-

tions [37]. Several contributions in the direction of such a unified approach were presented recently with respect to the heat current [32,35,37], whereas the power spectral density has not been considered. All in all, a better understanding of the behavior and the property of a quantum heat ratchet in this context remains a highly interesting challenge.

A. Integral principal value

In this appendix we derive Eq. (2.37) by using the definition of integral principle value. Plugging Eq. (2.35) into Eq. (2.20), we have

$$\begin{aligned} c_{\ell q}(t) =& \; c_{\ell q}(t_0)e^{-i\varepsilon_{\ell q}(t-t_0)/\hbar} - \frac{iV_{\ell q}}{\hbar}\int_{t_0}^{t} dt' e^{-i\varepsilon_{\ell q}(t-t')/\hbar}\sum_{\ell' q'}\frac{V^*_{\ell' q'}e^{-i\varepsilon_{\ell' q'}(t'-t_0)/\hbar}c_{\ell' q'}(t_0)}{\varepsilon_{\ell' q'}-\varepsilon_0+i(\Gamma_{\rm L}+\Gamma_{\rm R})/2} \\ =& \; c_{\ell q}(t_0)e^{-i\varepsilon_{\ell q}(t-t_0)/\hbar} - \frac{iV_{\ell q}}{\hbar}\sum_{\ell' q'}\frac{V^*_{\ell' q'}e^{i(\varepsilon_{\ell' q'}t_0-\varepsilon_{\ell q}t)/\hbar}c_{\ell' q'}(t_0)}{\varepsilon_{\ell' q'}-\varepsilon_0+i(\Gamma_{\rm L}+\Gamma_{\rm R})/2}\int_{t_0}^{t} dt' e^{-i(\varepsilon_{\ell' q'}-\varepsilon_{\ell q})t'/\hbar}. \end{aligned} \tag{A.1}$$

Now we need to complish the integral in the last step of Eq. (A.1).

$$\begin{aligned} \lim_{t_0\to-\infty}\int_{t_0}^{t} dt' e^{-i(\varepsilon_{\ell' q'}-\varepsilon_{\ell q})t'/\hbar} &= -\lim_{t_0\to-\infty}\int_{t-t_0}^{0} dt' e^{i(\varepsilon_{\ell' q'}-\varepsilon_{\ell q})t'/\hbar}e^{-i(\varepsilon_{\ell' q'}-\varepsilon_{\ell q})t/\hbar} \\ &= \lim_{t_0\to-\infty}\int_{0}^{t-t_0} dt' e^{i(\varepsilon_{\ell' q'}-\varepsilon_{\ell q})t'/\hbar}e^{-i(\varepsilon_{\ell' q'}-\varepsilon_{\ell q})t/\hbar} \\ &= \int_{0}^{\infty} dt' e^{i(\varepsilon_{\ell' q'}-\varepsilon_{\ell q})t'/\hbar}e^{-i(\varepsilon_{\ell' q'}-\varepsilon_{\ell q})t/\hbar}, \end{aligned} \tag{A.2}$$

where we have performed the substitution $t' \to t - t'$ and taken the initial time as $t_0 \to -\infty$. Now the task is to calculate the integral in the last step of Eq. (A.2):

$$\begin{aligned} \int_{0}^{\infty} dt' e^{i(\varepsilon_{\ell' q'}-\varepsilon_{\ell q})t'/\hbar} &= \lim_{\sigma\to 0^+}\int_{0}^{\infty} dt' e^{i(\varepsilon_{\ell' q'}-\varepsilon_{\ell q})t'/\hbar-\sigma t'/\hbar} \\ &= \lim_{\sigma\to 0^+}\frac{i\hbar}{\varepsilon_{\ell' q'}-\varepsilon_{\ell q}+i\sigma} \\ &= i\hbar\left(\frac{\mathcal{P}}{\varepsilon_{\ell' q'}-\varepsilon_{\ell q}} - i\pi\delta(\varepsilon_{\ell' q'}-\varepsilon_{\ell q})\right) \\ &= i\hbar B(\varepsilon_{\ell' q'}-\varepsilon_{\ell q}), \end{aligned} \tag{A.3}$$

where $\mathcal{P}(1/x) = \int_{-\infty}^{0^-} dx/x + \int_{0^+}^{\infty} dx/x$ (see Ref. [90]). Combining all the above results, we obtain Eq. (2.37).

A further property that is useful for those derivations containing with $B(E)$ is given by

$$B(E) = B^*(-E) \tag{A.4}$$

B. Derivation of the phonon transmission coefficient

We derive the phonon transmission coefficient of Eq. (3.21) along the lines of Ref. [38]. Starting with Eq. (33) of that work, which reads as

$$\begin{aligned}&(\omega_k^2 - \omega^2 + i\omega[\gamma_{k,k}^{\mathrm{L}}(\omega) + \gamma_{k,k}^{\mathrm{R}}(\omega)])A_k(\omega) \\ &+ i\omega \sum_{k' \neq k} \sqrt{\frac{\omega_k}{\omega_{k'}}}[\gamma_{k,k'}^{\mathrm{L}}(\omega) + \gamma_{k,k'}^{\mathrm{R}}(\omega)]A_{k'}(\omega) = \sqrt{\frac{\omega_k}{\omega}} V_{0,k} a^\dagger\end{aligned} \tag{B.1}$$

and assuming symmetric coupling, i.e.,

$$\gamma_{k,k'}^{\mathrm{L}}(\omega) = \gamma_{k,k'}^{\mathrm{R}}(\omega) = \gamma_{k,k'}(\omega) \ , \tag{B.2}$$

Eq. (33) of Ref. [38] can be simplified to read

$$\begin{aligned}&[\omega_k^2 - \omega^2 + 2i\omega\gamma_{k,k}(\omega)]A_k(\omega) \\ &+ i\omega \sum_{k' \neq k} \sqrt{\frac{\omega_k}{\omega_{k'}}} 2\gamma_{k,k'}(\omega)A_{k'}(\omega) = \sqrt{\frac{\omega_k}{\omega}} V_{0,k} a^\dagger \ .\end{aligned} \tag{B.3}$$

Since we only consider one phonon mode, i.e., $k = 1$, the second term on the left-hand side of Eq. (B.3) vanishes, such that

$$[\omega_1^2 - \omega^2 + 2i\omega\gamma_{1,1}(\omega)]A_1(\omega) = \sqrt{\frac{\omega_1}{\omega}} V_{0,1} a^\dagger. \tag{B.4}$$

Substituting Eq. (46) of Ref. [38], i.e.,

$$A_k(\omega) = \overline{A_k}(\omega) V_{0,k} a^\dagger \sqrt{\frac{\omega_k}{\omega}} \tag{B.5}$$

into Eq. (B.4), we find

$$\overline{A_1}(\omega) = \frac{1}{\omega_1^2 - \omega^2 + 2i\omega\gamma_{1,1}(\omega)} \ . \tag{B.6}$$

B. Derivation of the phonon transmission coefficient

For one phonon mode, the definition of the phonon transmission follows from Eq. (48) in Ref. [38],

$$\mathcal{T}(\omega) = \frac{2\omega^2}{\pi} \sum_{k,k'} \gamma^{\mathrm{R}}_{k,k'}(\omega)\gamma^{\mathrm{L}}_{k,k'}(\omega)[\overline{A_k}(\omega)\overline{A^\dagger_{k'}}(\omega) + \overline{A^\dagger_{k'}}(\omega)\overline{A_k}(\omega)]/2 \;, \tag{B.7}$$

which, however, differs from the commonly used definition given in e.g., Refs. [36, 82] by a factor $1/2\pi$. Using that common definition, the phonon transmission can be expressed as

$$\mathcal{T}(\omega) = 4\omega^2\gamma^2_{1,1}(\omega)|\overline{A_1}(\omega)|^2 \;. \tag{B.8}$$

Substituting Eq. (B.6) into Eq. (B.8) and omitting the subscript in $\gamma_{1,1}$, we obtain

$$\mathcal{T}(\omega) = \frac{4\omega^2\gamma^2(\omega)}{(\omega_1^2 - \omega^2)^2 + 4\omega^2\gamma^2(\omega)} \;, \tag{B.9}$$

which is the phonon transmission (3.21) employed in the main text.

References of previous work

[P1] N. Li, F. Zhan, P. Hänggi, and B. Li, *Shuttling heat across one-dimensional homogenous nonlinear lattices with a Brownian heat motor*, Phys. Rev. E **80**, 011125 (2009).

[P2] F. Zhan, N. Li, S. Kohler, and P. Hänggi, *Molecular Wires Acting as Quantum Heat Ratchet*, Phys. Rev. E **80**, 061115 (2009).

[P3] F. Zhan, S. Denisov, and P. Hänggi, *Electronic Heat Transport Across a Molecular Wire: Power Spectrum of Heat Fluctuations*, Phys. Rev. B (in press), arXiv: 1107.3434 (2011).

[P4] F. Zhan, S. Denisov, A. V. Ponomarev, and P. Hänggi, *Quantum ratchet transport with minimal dispersion rate*, Phys. Rev. A **84**, 043617 (2011).

Bibliography

[1] L. Wang and B. Li, *Phononics Gets Hot*, Phys. World **21**, 27 (2008).

[2] N. Li, J. Ren, L. Wang, G. Zhang, and P. Hänggi, *Phononics coming to life: manipulation nanoscale heat transport and beyond*, arXiv:1108.6120 (2011).

[3] M. Terraneo, M. Peyrard, and G. Casati, *Controlling the Energy Flow in Nonlinear Lattices: A Model for a Thermal Rectifier*, Phys. Rev. Lett. **88**, 094302 (2002).

[4] B. Li, L. Wang, and G. Casati, *Thermal Diode: Rectification of Heat Flux*, Phys. Rev. Lett. **93**, 184301 (2004).

[5] D. Segal and A. Nitzan, *Spin-Boson Thermal Rectifier*, Phys. Rev. Lett. **94**, 034301 (2005).

[6] B. Hu, L. Yang, and Y. Zhang, *Asymmetric Heat Conduction in Nonlinear Lattices*, Phys. Rev. Lett. **97**, 124302 (2006).

[7] M. Peyrard, *The Design of a Thermal Rectifier*, Europhys. Lett. **76**, 49 (2006).

[8] N. Yang, N. Li, L. Wang, and B. Li, *Thermal Rectification and Negative Differential Thermal Resistance in Lattices with Mass Gradient*, Phys. Rev. B **76**, 020301 (2007).

[9] D. Segal, *Single Mode Heat Rectifier: Controlling Energy Flow Between Electronic Conductors*, Phys. Rev. Lett. **100**, 105901 (2008).

[10] B. Li, L. Wang, and G. Casati, *Negative Differential Thermal Resistance and Thermal Transistor*, Appl. Phys. Lett. **88**, 143501 (2006).

[11] W. C. Lo, L. Wang, and B. Li, *Thermal Transistor: Heat Flux Switching and Modulating*, J. Phys. Soc. Jpn **77**, 054402 (2008).

[12] L. Wang and B. Li, *Thermal Logic Gates: Computation with Phonons*, Phys. Rev. Lett. **99**, 177208 (2007).

[13] L. Wang and B. Li, *Thermal Memory: A Storage of Phononic Information*, Phys. Rev. Lett. **101**, 267203 (2008).

[14] C. W. Chang, D. Okawa, A. Majumdar, and A. Zettl, *Solid-State Thermal Rectifier*, Science **314**, 1121 (2006).

[15] R. Scheibner, M. König, D. Reuter, A. D. Wieck, C. Gould, H. Buhmann, and L. W. Molenkamp, *Quantum Dot as Thermal Rectifier*, New J. Phys. **10**, 083016 (2008).

[16] N. Li, P. Hänggi, and B. Li, *Ratcheting Heat Flux Against a Thermal Bias*, EPL (Europhysics Letters) **84**, 40009 (2008).

[17] A. Nitzan and M. A. Ratner, *Electron Transport in Molecular Wire Junctions*, Science **300**, 1384 (2003).

[18] P. Hänggi, M. Ratner, and S. Yaliraki, *Transport in Molecular Wires*, Chem. Phys. **281**, 111 (2002).

[19] S. Kohler, J. Lehmann, and P. Hänggi, *Driven Quantum Transport on the Nanoscale*, Phys. Rep. **406**, 379 (2005).

[20] N. J. Tao, *Electron Transport in Molecular Junctions*, Nature Nanotech. **1**, 173 (2006).

[21] A. Aviram and M. A. Ratner, *Molecular Rectifiers*, Chem. Phys. Lett. **29**, 277 (1974).

[22] C. Joachim, J. K. Gimzewski, and A. Aviram, *Electronics Using Hybrid-Molecular and Mono-Molecular Devices*, Nature **408**, 541 (2000).

[23] M. A. Reed, C. Zhou, C. J. Muller, T. P. Burgin, and J. M. Tour, *Conductance of a Molecular Junction*, Science **278**, 252 (1997).

[24] J. Lehmann, S. Kohler, P. Hänggi, and A. Nitzan, *Rectification of Laser-Induced Electronic Transport through Molecules*, J. Chem. Phys. **118**, 3283 (2003).

[25] F. J. Kaiser and S. Kohler, *Shot Noise in Non-Adiabatically Driven Nanoscale Conductors*, Ann. Phys. (Leipzig) **16**, 702 (2007).

[26] M. Moskalets and M. Büttiker, *Dissipation and Noise in Adiabatic Quantum Pumps*, Phys. Rev. B **66**, 035306 (2002).

[27] F. Mohn, J. Repp, L. Gross, G. Meyer, M. S. Dyer, and M. Persson, *Reversible Bond Formation in a Gold-Atom–Organic-Molecule Complex as a Molecular Switch*, Phys. Rev. Lett. **105**, 266102 (2010).

[28] U. Sivan and Y. Imry, *Multichannel Landauer Formula for Thermoelectric Transport with Application to Thermopower near the Mobility Edge*, Phys. Rev. B **33**, 551 (1986).

[29] J. Koch, F. von Oppen, Y. Oreg, and E. Sela, *Thermopower of Single-Molecule Devices*, Phys. Rev. B **70**, 195107 (2004).

[30] Y.-C. Chen and M. Di Ventra, *Effect of Electron-Phonon Scattering on Shot Noise in Nanoscale Junctions*, Phys. Rev. Lett. **95**, 166802 (2005).

[31] M. Galperin, A. Nitzan, and M. A. Ratner, *Resonant Inelastic Tunneling in Molecular Junctions*, Phys. Rev. B **73**, 045314 (2006).

[32] M. Galperin, A. Nitzan, and M. A. Ratner, *Heat Conduction in Molecular Transport Junctions*, Phys. Rev. B **75**, 155312 (2007).

[33] D. Segal, *Heat Flow in Nonlinear Molecular Junctions: Master Equation Analysis*, Phys. Rev. B **73**, 205415 (2006).

[34] M. Paulsson and S. Datta, *Thermoelectric Effect in Molecular Electronics*, Phys. Rev. B **67**, 241403 (2003).

[35] M. Galperin, M. A. Ratner, and A. Nitzan, *Molecular Transport Junctions: Vibrational Effects*, J. Phys.: Condens. Matter **19**, 103207 (2007).

[36] J.-S. Wang, J. Wang, and J. T. Lü, *Quantum Thermal Transport in Nanostructures*, Eur. Phys. J. B **62**, 381 (2008).

[37] Y. Dubi and M. D. Ventra, *Heat Flow and Thermoelectricity in Atomic and Molecular Junctions*, Rev. Mod. Phys. **83**, 131 (2011).

[38] D. Segal, A. Nitzan, and P. Hänggi, *Thermal Conductance through Molecular Wires*, J. Chem. Phys. **119**, 6840 (2003).

[39] M. Rey, M. Strass, S. Kohler, P. Hänggi, and F. Sols, *Nonadiabatic Electron heat pump*, Phys. Rev. B **76**, 085337 (2007).

[40] M. Moskalets and M. Büttiker, *Floquet Scattering Theory for Current and Heat Noise in Large Amplitude Adiabatic Pumps*, Phys. Rev. B **70**, 245305 (2004).

[41] I. V. Krive, E. N. Bogachek, A. G. Scherbakov, and U. Landman, *Heat Current Fluctuation in Quantum Wires*, Phys. Rev. B **64**, 233304 (2001).

[42] D. Sergi, *Engergy Transport and Fluctuation in Small Conductors*, Phys. Rev. B **83**, 033401 (2011).

[43] D. V. Averin and J. P. Pekola, *Violation of the Fluctuation-Dissipation Theorem in Time-Dependent Msoscopic Heat Transport*, Phys. Rev. Lett. **104**, 220601 (2010).

[44] U. Kleinekathöfer, G. Li, S. Welack, and M. Schreiber, *Switching the Current through Model Molecular Wires with Gaussian Laser Pulses*, Europhys. Lett. **75**, 139 (2006).

[45] S. S. Bayin, *Mathematical Methods in Science and Engineering*, Wiley (2006).

[46] Y. M. Blanter and M. Büttiker, *Shot Noise in Mesoscopic Conductors*, Phys. Rep. **336**, 1 (2000).

[47] S. Camalet, S. Kohler, and P. Hänggi, *Shot-Noise Control in ac-Driven Nanoscale Conductors*, Phys. Rev. B **70**, 155326 (2004).

[48] S. Kohler and P. Hänggi, *Molecular Electronics: Ultrafast Stop and Go*, Nature Nanotech. **2**, 675 (2007).

[49] M. A. Reed and T. Lee (editors), *Molecular Nanoelectronics*, American Scientific, Stevenson Ranch, CA (2003).

[50] M. A. Reed and J. M. Tour, *Computing with Molecules*, Sci. Am. **282**, 86 (2000).

[51] P. J. Kuekes, D. R. Stewart, and R. S. Williams, *The Crossbar Latch: Logic Value Storage, Restoration, and Inversion in Crossbar Circuits*, J. App. Phys. **97**, 034301 (2005).

[52] C. Zhang, M.-H. Du, H.-P. Cheng, X.-G. Zhang, A. E. Roitberg, and J. L. Krause, *Coherent Electron Transport through an Azobenzene Molecule: A Light-Driven Molecular Switch*, Phys. Rev. Lett. **92**, 158301 (2004).

[53] J. Lehmann, S. Camalet, S. Kohler, and P. Hänggi, *Laser Controlled Molecular Switches and Transistors*, Chem. Phys. Lett. **368**, 282 (2003).

[54] J. Lehmann, S. Kohler, V. May, and P. Hänggi, *Vibrational Effects in Laser-Driven Molecular Wires*, J. Chem. Phys. **121**, 2278 (2004).

[55] G.-Q. Li, M. Schreiber, and U. Kleinekathöfer, *Coherent Laser Control of the Current through Molecular Junctions*, EPL **79**, 27006 (2007).

[56] I. Franco, M. Shapiro, and P. Brumer, *Robust Ultrafast Currents in Molecular Wires through Stark Shifts*, Phys. Rev. Lett. **99**, 126802 (2007).

[57] Z.-Q. Zhang, N. D. Lang, and M. D. Ventra, *Effects of Geometry and Doping on the Operation of Molecular Transistors*, App. Phys. Lett. **82**, 1938 (2003).

[58] A. Ghosh, T. Rakshit, and S. Datta, *Gating of a Molecular Transistor: Electrostatic and Conformational*, Nano. Lett. **4**, 565 (2004).

[59] F. Jiang, Y.-X. Zhou, H. Chen, R. Note, H. Mizuseki, and Y. Kawazoe, *Self-Consistent Study of Single Molecular Transistor Modulated by Transverse Field*, J. Chem. Phys. **125**, 084710 (2006).

[60] K. Xiao, Y.-Q. Liu, T. Qi, W. Zhang, F. Wang, J.-H. Gao, W.-F. Qiu, Y.-Q. Ma, G.-L. Cui, S.-Y. Chen, X.-W. Zhan, G. Yu, J.-G. Qin, W.-P. Hu, and D.-B. Zhu, *A Highly -Stacked Organic Semiconductor for Field-Effect Transistors Based on Linearly Condensed Pentathienoacene*, J. Am. Chem. Soc. **127**, 13281 (2005).

[61] Y.-M. Sun, Y.-Q. Liu, and D.-B. Zhu, *Advances in Organic Field-Effect Transistors*, J. Mater. Chem. **15**, 53 (2005).

[62] B.-Q. Xu, X.-Y. Xiao, X.-M. Yang, L. Zang, and N.-J. Tao, *Large Gate Modulation in the Current of a Room Temperature Single Molecule Transistor*, J. Am. Chem. Soc. **127**, 2386 (2005).

[63] P. Reimann, R. Bartussek, R. Häußler, and P. Hänggi, *Brownian Motors Driven by Temperature Oscillations*, Phys. Lett. A **215**, 26 (1996).

[64] R. D. Astumian and P. Hänggi, *Brownian Motors*, Phys. Today **55**, 33 (2002).

[65] P. Hänggi, F. Marchesoni, and F. Nori, *Brownian Motors*, Ann. Phys. **14**, 51 (2005).

[66] P. Reimann and P. Hänggi, *Introduction to the Physics of Brownian Motors*, Appl. Phys. A: Mater. Sci. Process. **75**, 169 (2002).

[67] P. Hänggi and F. Marchesoni, *Artificial Brownian motors: Controlling transport on the nanoscale*, Rev. Mod. Phys. **81**, 387 (2009).

[68] L. Arrachea, M. Moskalets, and L. Martin-Moreno, *Heat Production and Energy Balance in Nanoscale Engines Driven by Time-Dependent Fields*, Phys. Rev. B **75**, 245420 (2007).

[69] J. Luczka, R. Bartussek, and P. Hänggi, *White-Noise-Induced Transport in Periodic Structures*, Europhys. Lett. **31**, 431 (1995).

[70] P. Hänggi, R. Bartussek, P. Talkner, and J. Łuczka, *Noise-Induced Transport in Symmetric Periodic Potentials: White Shot Noise versus Deterministic Noise*, Europhys. Lett. **35**, 315 (1996).

[71] I. Goychuk and P. Hänggi, *Quantum Rectifiers from Harmonic Mixing*, Europhys. Lett. **43**, 503 (1998).

[72] S. Flach, O. Yevtushenko, and Y. Zolotaryuk, *Directed Current due to Broken Time-Space Symmetry*, Phys. Rev. Lett. **84**, 2358 (2000).

[73] S. Denisov, S. Flach, A. A. Ovchinnikov, O. Yevtushenko, and Y. Zolotaryuk, *Broken Space-Time Symmetries and Mechanisms of Rectification of ac Fields by Nonlinear (Non)adiabatic Response*, Phys. Rev. E **66**, 041104 (2002).

[74] J. Lee, A. O. Govorov, and N. A. Kotov, *Nanoparticle Assemblies with Molecular Springs: A Nanoscale Thermometer*, Angew. Chem. Int. Ed. **44**, 7439 (2005).

[75] R. H. M. Groeneveld, R. Sprik, and A. Lagendijk, *Femtosecond spectroscopy of electron-electron and electron-phonon energy relaxation in Ag and Au*, Phys. Rev. B **51**, 11433 (1995).

[76] N. Del Fatti, C. Voisin, M. Achermann, S. Tzortzakis, D. Christofilos, and F. Vallée, *Nonequilibrium electron dynamics in noble metals*, Phys. Rev. B **61**, 16956 (2000).

[77] R. Knorren, K. H. Bennemann, R. Burgermeister, and M. Aeschlimann, *Dynamics of excited electrons in copper and ferromagnetic transition metals: Theory and experiment*, Phys. Rev. B **61**, 9427 (2000).

[78] P. J. van Hall, *Ultrafast processes in Ag and Au: A Monte Carlo study*, Phys. Rev. B **63**, 104301 (2001).

[79] J. P. Girardeau-Montaut, M. Afif, C. Girardeau-Montaut, S. D. Moustaïzis, and N. Papadogiannis, *Aluminium electron-phonon relaxation-time measurement from subpicosecond nonlinear single-photon photoelectric emission at 248 nm*, Appl. Phys. A: Mater. Sci. Process. **62**, 3 (1996).

[80] M. van Kampen, J. T. Kohlhepp, W. de Jonge, B. Koopmans, and R. Coehoorn, *Sub-picosecond electron and phonon dynamics in nickel*, J. Phys.: Condens. Matter **17**, 6823 (2005).

[81] X. Zheng, W. Zheng, Y. Wei, Z. Zeng, and J. Wang, *Thermoelectric Transport Properties in Atomic Scale Conductors*, J. Chem. Phys. **121**, 8537 (2004).

[82] L. G. C. Rego and G. Kirczenow, *Quantized Thermal Conductance of Dielectric Quantum Wires*, Phys. Rev. Lett. **81**, 232 (1998).

[83] A. Ozpineci and S. Ciraci, *Quantum Effects of Thermal Conductance through Atomic Chains*, Phys. Rev. B **63**, 125415 (2001).

[84] J. Grunenberg, *Intrinsic Bond Strengths of Multiple CC, SiSi, and CSi Bonds*, Angew. Chem. Int. Ed. **40**, 4027 (2001).

[85] Z.-H. Wang, J. A. Carter, A. Lagutchev, Y. K. Koh, N.-H. Seong, D. G. Cahill, and D. D. Dlott, *Ultrafast Flash Thermal Conductance of Molecular Chains*, Science **317**, 787 (2007).

[86] P. Reimann, M. Grifoni, and P. Hänggi, *Quantum Ratchets*, Phys. Rev. Lett. **79**, 10 (1997).

[87] H. Linke, T. E. Humphrey, A. Löfgren, A. O. Sushkov, R. Newbury, R. P. Taylor, and P. Omling, *Experimental Tunneling Ratchets*, Science **286**, 2314 (1999).

[88] I. Terasaki, Y. Sasago, and K. Uchinokura, *Large thermoelectric power in* NaCo_2O_4 *single crystals*, Phys. Rev. B **56**, R12685 (1997).

[89] H. B. Callen, *Thermodynamics and an introduction to thermostatics*, Wiley, New York, second edn. (1985), see Secs. 14.5-14.9 therein.

[90] V. S. Vladimirov, *Equations of Mathematical Physics*, Dekker, New York (1971).

Acknowledgement

First of all, I would like to express my gratitude to Prof. Dr. Peter Hänggi and Prof. Dr. Sigmund Kohler for giving me the invaluable opportunity to join the group of Theoretische Physik I at Institut für Physik, Universität Augsburg. Moreover, they offered me this interesting project on *Quantum transport at the molecular scale*. During my PhD studies, I have profited a lot from their constant support, their broad knowledge and experience. I would also like to thank both of them for being the referees of this thesis.

I also would like to express my thanks to Prof. Dr. Achim Wixforth and Dr. Peter Schwab for being board members of my PhD defense committee. In addition, I would like to express my appreciation to Privatdozent Dr. Stefan Ludwig for being my second supervisor in the framework of the Graduate Program organized by Nanosystems Initiative Munich (NIM). His helpful introduction and our discussions about experimental aspects of quantum dots helped me a lot to expand my understanding of this matter. I would also like to acknowledge financial support by the Deutsche Forschungsgemeinschaft (DFG) within the Schwerpunktprogramm SPP 1243.

My special thanks go to Dr. Nianbei Li, Dr. Alexey Ponomarev, and Dr. Sergey Denisov. I enjoyed a lot our discussions about physics, future research plans, and both theoretical and numerical methods to support my research. Moreover, I am deeply indebted to them for their support regarding my publications. With respect to the preparation of this thesis, I would like to acknowledge the valuable assistance of Dr. Georg Reuther, Dr. Michele Campisi, Dr. Alexey Ponomarev, and Dr. Sergey Denisov for proofreading the manuscript.

In July and August of 2010, I participated in the NIM summer research program as a mentor. This allowed me to gain a wonderful teaching experience together with my summer student. I would like to thank Dr. Wolfgang Häusler for our collaboration and his support within this this program.

Furthermore, I would like to thank all former and present colleagues of the "Theo 1" group for offering me a very nice and stimulating research environment. Especially I would like to thank Dr. Peter Siegle, Dr. Philippe Beltrame, Dr. Nianbei Li, and Dr. Michele Campisi, with whom I shared the office during the three years and had many interesting and fruitful discussions. For all her services concerning "initial problems" such as finding an apartment, registering as a student at Augsburg University, organizing visa, and many more, I would like

to express my special appreciation to our secretary Frau Eva Seehuber. In this connection I also would like to thank Dr. Jun Lu, who helped me to get used to the life in Augsburg especially in the first few months after my arrival, and Dr. Sebastian Deffner, the organizer of the unforgettable bier sessions. I also thank Dr. Georg Reuther, Dr. Sebastian Deffner, and Dr. Andereas Sinner for constantly helping me to improve my knowledge of the German language.

For broad support regarding computer usage, software and the cluster service in the institute, I would like to thank Ralf Utermann, Prof. Dr. Gert-Ludwig Ingold, Dr. Gerhard Schmid, and Dr. Georg Reuther.

Last but not least, I am very grateful to my family and to my wife Ensi for supporting me during all the time, even over a great distance. It is especially my parents who have always been convinced that I will pursue a successful scientific career.

Lebenslauf

Name:	Zhan, Fei
Geburtsdatum:	17. Juli 1982
Geburtsort:	Xintai, Shandong, China
Familienstand:	verheiratet mit Liu, Ensi

September 1998 - Juli 2001	Gymnasium Xinwen, Shandong, China
September 2001 - Juli 2005	Bachelor Physik, Shandong Universität, Jinan, Shandong, China
September 2005 - Juni 2008	Master Physik, Institut für Physik, Chinesische Akademie der Wissenschaften, Peking, China
Seit September 2008	Wissenschaftlicher Mitarbeiter, Universität Augsburg